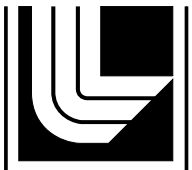

LAWRENCE
LIVERMORE
NATIONAL
LABORATORY

UCRL-JRNL-215158

South Asian Summer Monsoon and Its Relationship with ENSO in the IPCC AR4 Simulations

H. Annamalai, K. Hamilton, K. R. Sperber

September 8, 2005

Journal of Climate

South Asian Summer Monsoon and Its Relationship with ENSO in the IPCC AR4 simulations

H. Annamalai[@*], K. Hamilton[*], and K. R. Sperber[+]

[*] International Pacific Research Center, University of Hawaii, Honolulu, Hawaii

[+]PCMDI, Lawrence Livermore National Laboratory, Livermore, California.

J. Climate (revised)

June 2006

@ Corresponding Author: Dr. H. Annamalai, IPRC/SOEST, University of Hawaii, 1680 East West Road, Honolulu, HI 96822, USA. Email: hanna@hawaii.edu

Abstract

In this paper we use the extensive integrations produced for the IPCC Fourth Assessment Report (AR4) to examine the relationship between ENSO and the monsoon at interannual and decadal timescales. We begin with an analysis of the monsoon simulation in the 20th century integrations. Six of the 18 models were found to have a reasonably realistic representation of monsoon precipitation climatology. For each of these six models SST and anomalous precipitation evolution along the equatorial Pacific during El Niño events display considerable differences when compared to observations. Out of these six models only four (GFDL_CM_2.0, GFDL_CM_2.1, MRI, and MPI_ECHAM5) exhibit a robust ENSO-monsoon contemporaneous teleconnection, including the known inverse relationship between ENSO and rainfall variations over India. Lagged correlations between the all-India rainfall (AIR) index and Nino3.4 SST reveal that three models represent the timing of the teleconnection, including the spring predictability barrier which is manifested as the transition from positive to negative correlations prior to the monsoon onset. Furthermore, only one of these three models (GFDL_CM_2.1) captures the observed phase lag with the strongest anticorrelation of SST peaking 2-3 months after the summer monsoon, which is partially attributable to the intensity of simulated El Niño itself. We find that the models that best capture the ENSO-monsoon teleconnection are those that correctly simulate the timing and location of SST and diabatic heating anomalies in the equatorial Pacific, and the associated changes to the equatorial Walker Circulation during El Niño events.

The strength of the AIR-Nino3.4 SST correlation in the model runs waxes and wanes to some degree on decadal timescales. The overall magnitude and timescale for this decadal modulation in most of the models is similar to that seen in observations. However, there is little consistency in

the phase among the realizations, suggesting a lack of predictability of the decadal modulation of the monsoon-ENSO relationship.

The analysis was repeated for each of the four models using results from integrations in which the atmospheric CO_2 concentration was raised to twice pre-industrial values. From these "best" models in the double CO_2 simulations there are increases in both the mean monsoon rainfall over the Indian sub-continent (by 5-25%) and in its interannual variability (5-10%). We find for each model that the ENSO-monsoon correlation in the global warming runs is very similar to that in the 20^{th} century runs, suggesting that the ENSO-monsoon connection will not weaken as global climate warms. This result, though plausible, needs to be taken with some caution because of the diversity in the simulation of ENSO variability in the coupled models we have analyzed. The implication of the present results for monsoon prediction are discussed.

1. Introduction

One of the major components of the Asian Summer Monsoon (ASM) is the Indian Summer Monsoon whose strength is often represented by the all-India Rainfall (AIR) index (Parthasarathy et al. 1994). The AIR index represents the area-weighted seasonal average (June-September) rainfall over continental India. Despite its remarkable regularity each year, the monsoon does exhibit substantial variability at subseasonal and interannual time-scales (Webster et al. 1998; Annamalai et al. 1999), exerting profound social and economical consequences over the heavily populated regions.

Since the seminal work of Walker and Bliss (1932) it has been appreciated that contemporaneous SST anomalies in the central-eastern Pacific associated with El Niño-Southern Oscillation (ENSO) have been the predominant forcing of the AIR index variability (e.g., Sikka 1980; Shukla and Paolino 1983; Rasmusson and Carpenter 1983; Nigam 1994; Meehl and Arblaster 2002; Annamalai and Liu 2005). This suggests that there may be potential predictability of the mean monsoon and its interannual variability through the influence of slowly varying boundary conditions (Charney and Shukla 1981). Through the 1980's the tendency for below-normal (above-normal) AIR to occur during El Niño (La Nina) was generally observed. The picture became somewhat more complicated when the ENSO-monsoon relationship during the 1990s' was observed to be weaker than in the previous decades (Shukla 1995; Kinter et al. 2002). It has been suggested that the weakened ENSO-monsoon relationship may be partially attributable to global warming (Krishnakumar et al. 1999). However, there is also evidence that the strength of this linkage varies on decadal time scales (e.g., Parthasarathy et al. 1991). Recently, the deficit of AIR (19% and 13% below normal) that has occurred during the moderate El Niño events of 2002 and 2004 raises the question whether this relationship is again strengthening and returning to the

state that dominated before the 1990's. This is an important question since our ability to forecast ENSO up to one year in advance has shown increasing skill in recent years (e.g., Latif et al. 1998). If the monsoon-ENSO relationship remains reasonably constant in the future, this provides hope that interannual fluctuations of the monsoon may be at least partially predictable. Alternatively, if this relationship fails, then the leading indicator of year-to-year monsoon variability will be lost.

Though some model studies find little impact on AIR in climate change experiments (Mahfouf et al. 1994; Timbal et al. 1995), others find increased Indian monsoon rainfall relative to control simulations (Meehl and Washington 1993; Meehl and Arblaster 2003; Hu et al. 2000; May 2002). The robustness of the monsoon-ENSO relationship has varied among these global warming studies. A striking example of conflicting results regarding the ENSO-monsoon relationship in global warming simulations is provided by the work of Ashrit et al. (2001; 2003; 2005). In their 2001 paper the ENSO-monsoon relationship remained essentially intact, though it weakened slightly due to a declining impact during El Niño. Ashrit et al. (2003) found no "systematic change" in the ENSO-monsoon relationship, while in their 2005 paper the relationship was found to lose statistical significance after 2050.

There are numerous factors that may help produce the diversity of results, including (1) the quality of the simulated of mean monsoon precipitation in each model and (2) the fidelity with which the observed monsoon-ENSO relationship is represented in the control experiments. With respect to item (1), the diversity in the monsoon response noted in different climate models led Shukla (1984) to hypothesize that the realistic anomalous response depends on the models' ability to simulate the mean monsoon circulation and precipitation in the control experiments, a point further emphasized by Fennessy et al. (1994). Sperber and Palmer (1996) demonstrated that models with a more realistic mean state tended to better represent the interannual variability of AIR

related to ENSO. Subsequently, Sperber (1999) found that model improvement increased skill in this respect. Recent studies confirm the hypothesis that improvements in a model's mean climatology generally leads to a more realistic simulation of the monsoon response to ENSO forcing (Lau and Nath 2000; Annamalai and Liu 2005).

In the case of item (2), coupled models are known to differ significantly in their basic ability to simulate ENSO (Latif et al. 2001; AchutaRao and Sperber 2002), which of course has a direct bearing on the simulated monsoon-ENSO relationship. The future behavior of the ENSO-monsoon association will presumably depend also on how ENSO characteristics change in a warmer climate. Most global warming experiments have produced an "El Niño-like" time-mean change in the tropical Pacific SST and overlying atmospheric circulation (e.g., Knutson and Manabe 1994; 1995; Meehl et al. 2001), but more conflicting results for the changes in the behavior of ENSO itself have been found. For example, while Knutson and Manabe (1994) found a decrease in the amplitude of ENSO variations in a warmer climate, Meehl and Arblaster (2003) noted an increase.

The availability of the simulations with numerous contemporary global coupled models conducted recently for the IPCC AR4 allows for analysis of the historical and projected variations in ENSO-monsoon coupling. Initial analysis of these new integrations has shown that the current state-of-the art models show significant improvement in many aspects of ENSO compared to the previous generation of models (AchutaRao and Sperber 2006; Joseph and Nigam 2006; Guilyardi, 2006). Importantly, Turner et al. (2005) have demonstrated that improvement in representing the mean state of the tropical Pacific through the use of flux adjustment gave rise to a more realistic ENSO, which in turn improved the monsoon-ENSO relationship in the HadCM3 model. These

results indicate that the items above are a critical (though not necessarily sufficient) condition for generating a realistic monsoon-ENSO teleconnection.

In this paper we present an analysis of the ENSO-monsoon relationship in retrospective integrations as well as future climate change forecast runs of coupled models in the AR4 database. We will concentrate on those models that have the most realistic present-day representation of (i) mean monsoon precipitation climatology, (ii) ENSO characteristics, and (iii) the ENSO-monsoon relationship at interannual and decadal time scales.

The paper is organized as follows. Section 2 provides a brief description of the models. Section 3 presents the mean monsoon and ENSO in the control experiments. In Section 4, the surface temperature and monsoon responses in climate change experiments are presented. Section 5 deals with the ENSO-monsoon relationship. Section 6 provides the summary and conclusions.

2. The Models and Observations

Table 1 contains basic information with regard to the experimental notation and IPCC model configurations used in this paper. Numerous modelling groups submitted data from more than one model version. The two GFDL models differ in their dynamical core, cloud scheme, and land model. The atmosphere and ocean component models in GISS-AOM differ from those of GISS-EH and GISS-ER. These latter two models only differ in the choice of ocean model. The MIROC models employ the same physics, but are configured at different horizontal and vertical resolutions. From the National Center for Atmospheric Research (NCAR) results were submitted from the Parallel Climate Model (PCM), which was also used in CMIP2, and from the Community Climate System Model Version 3 (CCSM3). The UK Met Office simulations include HadCM3 as well as their lat-

est coupled model, HadGEM1. More detailed online model documentation for the IPCC models is available at:

http://www-pcmdi.llnl.gov/ipcc/model_documentation/ipcc_model_documentation.php

We have examined the output of 18 models used to simulate the climate of the 20th Century (20c3m) as part of the IPCC AR4. The 20c3m simulations attempt to replicate the overall climate variations during the period ~1850-present by imposing each modelling groups best estimates of natural (e.g., solar irradiance, volcanic aerosols) and anthropogenic (e.g., greenhouse gases, sulfate aerosols, ozone) climate forcing during this period. For each of these models multiple realizations of the 20th century simulations were used to evaluate the mean monsoon and the monsoon-ENSO relationship. For those models that do an adequate job of simulating these aspects of climate variability in the 20c3m runs, we will proceed to examine the monsoon and ENSO behavior in global warming experiments. Specifically we will analyze the "1pctto2x" experiments which impose a 1%/year CO_2 increase to doubling of initial concentration (~70 years) and then hold the CO_2 constant for an additional ~150 years of simulation. We will analyze only the period in the run after the CO_2 has been stabilized at twice the pre-industrial day value. Due to the limited amount of high frequency (daily/pentad) data available from the 1pctto2x simulations (~20 years), our analysis of temporal evolution of pentad rainfall over south Asia also includes output from the SRESA1B simulations, in which the concentration of greenhouse gases is changed over the period up to 2100 in accordance with plausible emission scenarios (by 2100 the CO_2 concentration is 720 ppmv). The 2100 greenhouse concentrations were then fixed for extended integrations of 100 or more years.

The observed all-India Rainfall (AIR) index is that of Parthasarathy et al. (1994). The AIR is constructed based on 306 quality-controlled stations spread over the whole of the Indian sub-

continent. For validating the spatial pattern of the time-mean rainfall we use the Climate Prediction Center Merged Analysis of Precipitation (CMAP) data set of Xie and Arkin (1996). We will also use the observed sea surface temperature from the Hadley Centre Ice/SST data set (HadISST; Rayner et al. 2003). We also use the recent 1^{o}x1^{o} gridded observed rainfall data over India produced by the India Meteorological Department (Rajeevan et al. 2005).

3. Mean Monsoon and ENSO in the 20c3m simulations

(a) Mean Monsoon Precipitation

The simulation of monsoon precipitation climatology has proven to be rather difficult and therefore provides a severe test of the climate models. As a first step, the seasonal average (June - September) precipitation climatology was constructed from the last 30-years (1971-2000 or 1970-99) of the 20c3m simulations for each of the 18 models. Observations (Fig. 1g) indicate that over the ASM region, intense precipitation occurs over three regions that represent: (i) the Indian Summer Monsoon (ISM, 10^{o}N-25^{o}N, 70^{o}E-100^{o}E), (ii) the Western North Pacific Monsoon (WNPM, 10^{o}N-20^{o}N, 110^{o}E-150^{o}E), and (iii) the eastern equatorial Indian Ocean (EEIO, 10^{o}S-0, 90^{o}E-110^{o}E). A realistic representation of these three centers is important in order to adequately investigate the variability of the ISM because these centers do not respond in unison to ENSO forcing, and the convective variabilities over the EEIO and WNPM modulate the ISM at interannual time scales (Annamalai and Liu 2005). Also at intraseasonal time scales these three centers mutually influence each other (Annamalai and Sperber 2005).

Our criteria for retaining a model for further investigation in this study thus requires a measure of fidelity at simulating the JJAS rainfall climatology, both over India (since we are using AIR; 65-95^{o}E, 7^{o}N-30^{o}N) and for the larger monsoon domain (40-180^{o}E, 25^{o}S-40^{o}N), to repre-

sent the three major convection centers. The selection metrics we use, pattern correlations and root mean square differences (RMSDs) relative to the observed precipitation estimates for the period 1979-2003, are noted in Fig. 1. Only 6 out of 18 models have larger pattern correlation and smaller RMSD with observations, and the statistics exceed 95% confidence level. This approach is consistent with past experience in which prescribed observed SST simulations with a realistic AIR-ENSO teleconnection have much higher pattern correlations of JJAS climatological precipitation over India, typically 0.6-0.7, than do simulations with a poor AIR-ENSO teleconnection (Sperber 1999). Importantly, these six models also represent well the afore-mentioned three centers of intense precipitation as indicated by pattern correlations of 0.7-0.8 over the broader ASM domain (Fig. 1). More detailed analysis is focussed on these six models, while the ENSO-monsoon diagnostics for other models are briefly mentioned in Section 5d.

Of the six models, both versions of the GFDL model produce simulations of ASM region rainfall with highest pattern correlation and lowest RMSD relative to observations. Yet, some significant systematic errors still exist in these models. For example, the precipitation strength over the EEIO (Figs. 1a, b) is comparable to or even greater than that over the ISM region. Also, the models have difficulty in capturing the regional details in precipitation over India, in particular, the high rainfall along the west coast. Furthermore, an examination of the monthly precipitation evolution over the monsoon domain (Fig. 1h) reveals that compared to observations, the intensity of the simulated precipitation during June-September is systematically weaker in all the models. Although they faithfully represent the transition phase from May to June, the timing of the peak rainfall varies considerably among the models. In terms of the annual cycle, the simulation from the MRI appears to be most realistic.

(b) ENSO Characteristics

Prior to evaluating the monsoon-ENSO relationship, we need to evaluate the quality of ENSO in these models, in particular the space-time evolution of SST, and associated precipitation anomalies along the equatorial Pacific, and the resultant circulation anomalies that link the tropical Pacific to the monsoon domain. Figure 2a shows the composite evolution of Nino3.4 SST anomalies during El Niño events in the six models. The composites are based on strong El Niño events (Nino3.4 SST exceeding 1.0 standard deviation during the monsoon season) from the first member of the ensemble. In agreement with observations (thick line) the typical life cycle of El Niño events in the models too is about 2 years. With the exception of NCAR_PCM the models capture the observed phase of ENSO, peaking in boreal winter. However, there is diversity in the amplitude compared to observations particularly in boreal summer that may impact the strength of the monsoon-ENSO relationship, as will be demonstrated later.

The spatial evolution of tropical Pacific SST and precipitation anomalies is a crucial element for determining the fidelity of a model ENSO. It is well known that during El Niño the eastward movement of the warmest SSTs (Fig. 3a), is accompanied by an eastward migration of convection into the central Pacific and a suppression of convection over the Maritime Continent (Fig. 4a). During El Niño years, the redistribution of latent heat sources and sinks in the equatorial Pacific determines the rising/descending branches of the anomalous Walker Circulation, the most important element in the ENSO-monsoon teleconnection. This is evident in 200hPa velocity potential anomalies (Fig. 5a) in which changes in the Walker Circulation induce large-scale subsidence over India, resulting in weaker monsoons. We now examine the representation of these simple diagnostics in the models.

For the sake of brevity we show the diagnostics from only 2 of the 6 models, NCAR_PCM and GFDL _CM_2.1 (Figs. 3-5). Noting that NCAR_PCM did not capture the observed phase-locking of Nino3.4 SST anomalies with the seasonal cycle (Fig. 2a), we also find that it does not have an ENSO cycle that develops as in observations. The warm SST signal, SSTs > 27.5^{o}C (a temperature sometimes used as the threshold associated with the occurrence of deep convection in the tropics), has not developed in the western-central Pacific (Fig. 3b), the precipitation anomalies develop incorrectly from the east (Fig. 4b) and the associated divergent outflow over the Pacific Ocean is shifted eastwards and is also very weak (Fig. 5b). As will be seen, these shortcomings adversely affect the ability of NCAR_PCM to simulate the monsoon-ENSO teleconnection. Conversely, GFDL_CM_2.1 simulates well these aspects of El Niño, but the strength of the simulated anomalies are much stronger than in observations (Figs. 3c, 4c, and 5c). It is notable that the model simulates the reduction in rainfall over the Maritime Continent despite the presence of quite warm SSTs there (Fig. 4c). The simulation of reduced precipitation over this region from boreal spring onwards reflects the effect of large-scale subsidence induced by the anomalous Walker Circulation (Fig. 5c). The HadCM3, like the PCM, does not simulate the observed negative precipitation anomalies over the Maritime Continent (not shown), while the simulated SST and precipitation anomalies along the entire equatorial Pacific are too intense and persist for more than a year in MPI (not shown). In GFDL_CM_2.0 and MRI, the simulated aspects of El Niño are closer to observations (not shown). In all the six models, however, warm SST anomalies and associated enhanced precipitation extend well into the equatorial west Pacific.

Our diagnostics of model ENSO are consistent with more detailed analysis carried out by others. Joseph and Nigam (2006) investigated the aspects of ENSO in 20c3m integrations with 3 of the 6 models examined here. They too noted large diversity in the amplitude of simulated

Nino3.4 SST anomalies, and in the spatial structure of SST and precipitation anomalies over the tropical Pacific (see Figs. 1,4 and 5 of their paper). AchutaRao and Sperber (2006) analyzed the representation of ENSO in control simulations with 19 of the AR4 models. They composited spatial patterns of surface temperature anomalies in the boreal winter peak phase for simulated El Niño events, and compared them to observed composites. Based on this diagnostic, it turns out that the 6 models we have selected as having the best ASM rainfall simulations are among the 8 best models in terms of their El Niño surface temperature composite.

In summary, even in these "best" models, systematic errors do exist in the simulation of mean monsoon precipitation and ENSO characteristics. These caveats are taken into account while interpreting the monsoon's response to global warming and in the ENSO-monsoon diagnostics (Section 5).

4. Surface Temperature, and Monsoon response in the 1pctto2x integrations

Figure 6 shows the seasonal mean (June-September) difference in surface temperature between the 1pctto2x and 20c3m integrations. In all the models the increase in surface temperature over the land is larger than over the oceans, consistent with results from many earlier global warming model experiments. The land-sea thermal contrast between the Eurasian continent and tropical Indian Ocean, which is an important aspect of the forcing driving the large-scale monsoon circulation particularly during the onset stages in May-June, increases in the 1pctto2x experiments by about 2-3^{o}C during June-September. During the pre-monsoon season (March-May, not shown) the rise in this thermal contrast is in the order of 3-4^{o}C. The southern tropical Indian Ocean which is a major moisture source, too shows an increase of SST in the 1pctto2x experiments. From sensitivity experiments with AGCMs, Ju and Slingo (1995), and Soman and Slingo

(1997) demonstrated that a small rise in SST over the tropical west Pacific warm pool has a large impact on the monsoon, with warmer and moister conditions favoring increased monsoon rainfall.

In addition to the overall warming and moistening of the atmosphere, and the enhanced regional-scale land-sea temperature contrast, the monsoon rainfall in the global warming simulation may be affected by the larger-scale changes in SST and the overlying atmospheric circulation. Inspection of Fig. 6 indicates that the zonal SST gradient in the equatorial Pacific is systematically reduced in the models, except in NCAR_PCM. The implication is that the "time-averaged" response of the tropical Pacific SST to an increase in CO_2 concentration takes the form of an El Niño-like pattern, consistent with results from many earlier model studies (e.g., Knutson and Manabe 1994; Meehl et al. 2001). Given the observed inverse relationship between El Niño and monsoon rainfall, one might expect this modulation of the large-scale SST gradient in the Pacific to contribute to a reduction in monsoon precipitation in the 1pctto2x integrations. In summary, two competing mechanisms for modulating monsoon rainfall are present in the 1pctto2x experiments (i) the overall warming and the enhanced land-sea surface temperature contrast that are expected to act to increase monsoon rainfall, while (ii) the larger-scale modulation of SST in the tropical Pacific may be expected to reduce the monsoon precipitation.

The spatial pattern of mean precipitation and the interannual standard deviations in the 1pctto2x experiments (not shown) remain similar overall to that shown from 20c3m integrations (Fig. 1). Figure 7 presents the differences in precipitation climatology and standard deviations between the 1pctto2x and 20c3m simulations. An important result is that the six models predict an increase (in the range 5-25%) in monsoon precipitation over the Indian sub-continent, as well as an increase in variability (5-10%). Yukimoto et al. (2005) also note an increase in rainfall over India in the SRESA1B simulations compared to the 20c3m runs. It should be mentioned here that

the increase in mean precipitation over India and its neighborhood is significant at 90% level except in MRI where the significance exceeds 95% level. To further investigate this, we estimated the changes in mean and variability of AIR index (Table 2) for four models that have realistic representation of ENSO-monsoon relationship (Section 5). We note that the changes are statistically significant for the AIR index. The future projection of mean precipitation and its variability over the other two major centers, namely over the WNPM and EEIO, are complex and varied (Fig. 7). Away from the WNPM and EEIO regions, five of the models forecast an increase in precipitation and its variability along the East Asian monsoon front that resides over Korea and Japan, with only the NCAR_PCM being an exception. The actual mechanisms involved in the time-mean precipitation response in the 1pctto2x runs will be analyzed further and presented in a future article.

As noted above the increase in land-sea thermal contrast in the 1pctto2x runs can be expected to contribute to an increase in monsoon rainfall, but it could also affect the timing of monsoon rains. In Fig. 8 we show the temporal evolution of the pentad mean precipitation averaged over the south Asian monsoon region (60^{o}E-100^{o}E, 5^{o}N-25^{o}N), both from the 20c3m and the perturbation runs for the two models that have the smallest (GFDL_CM_2.0) and largest (MRI) increase in the land-sea thermal contrast (Fig. 6). For comparison, we show the observations from two versions of CMAP and the GPCP analysis. The CMAP and GPCP have a very similar time evolution of the rainfall, but the GPCP values are generally about 10-20% lower than those computed from CMAP. The lower rainfall amounts over the ocean in GPCP occur because, in terms of absolute amount, the GPCP data were not tied as closely to atoll gauge estimates, which were believed to be an overestimate of rainfall over the open ocean (G. Huffman 2000, personal communication). In CMAP, there is an increase of rainfall of about 2.0 mm/day in the beginning of April and May (pentads 19 and 25) but during the monsoon onset (end of May) there

is a sudden increase of rainfall in the order of about 5.0 mm/day. The peak phase of the monsoon occurs in June-July. In the 20c3m runs the GFDL model (thick blue line in Fig. 8a) has a late onset compared to observations, but the MRI model results (thick blue line in Fig. 8b) agree rather well with GPCP. In the global warming perturbation experiment (brown line in Fig. 8a), the onset in the GFDL model occurs even later than in the 20c3m results, with increased rainfall during the later part of the monsoon season. The figure also shows results for the SRESA1B runs for different periods throughout the last 250 years of the experiment. For GFDL there does not seem to be a significant change in behavior with time. By contrast, the MRI model shows a systematic trend of greater monsoon rainfall as global warming progresses, with an earlier onset by 2-3 pentads compared to the 20c3m run, consistent with the larger four-month mean increase noted in Fig. 7d.

In the 1pctto2x runs evolution of total SST and anomalous precipitation along the equator composited over all El Niño years with the GFDL_CM_2.1 model (not shown) indicate the SST evolution in these runs is very similar to that in the 20c3m runs (Fig. 3c), except for the overall SST increase. The overall warming and change in the mean east-west SST gradient (Fig. 6b) results in the region with SSTs > 27.5^{o}C expanding further eastwards into the eastern Pacific during the pre-monsoon season. However, the anomalous precipitation in the El Niño composite for the 1pctto2x experiment is very similar to that in the 20c3m runs (Fig. 4c). Barring changes in intensity, the evolution of Nino3.4 SST anomalies from the 1pctto2x runs (Fig. 2b) also remain similar to those in 20c3m runs (Fig. 2a). Both MRI and MPI show systematic increase in El Niño intensity, while GFDL_CM_2.1 indicates otherwise (Fig. 2b).

5. ENSO-monsoon relationship

(a) Role of ENSO on the monsoon

As mentioned above, the 6 models analyzed here were chosen for their reasonable simulations of time-mean precipitation over the monsoon region. Our next step is to examine the monsoon-ENSO teleconnection in the 20c3m simulations. In particular, we plot correlation coefficients of the SST throughout the tropical Pacific and Indian Ocean region with the AIR rainfall index (to be consistent with the observations, the AIR index for the model results is constructed using only the land points over the region 7^{o}N-30^{o}N, 65^{o}E-95^{o}E). For each of the six models, this correlation is calculated separately for each realization, and then an ensemble-mean pattern is computed. The teleconnection patterns computed from the individual ensemble members (not shown) show similar features as the ensemble means. Figures 9 (b-f) show the ensemble correlation patterns between the seasonal mean AIR and SST from five of the models. Except for the NCAR_PCM (Fig. 9f) and HadCM3 (not shown), the models exhibit a robust teleconnection pattern similar to observations (Fig. 9a). The GFDL_CM_2.1 and MRI models best capture the negative correlations in the central/eastern Pacific, despite large differences in the simulated intensity of ENSO between them (Fig. 2a). In all the models, an apparent systematic error is the westward penetration of the negative correlations along the equatorial Pacific. This is consistent with the tendency of the models to have the El Niño warming extend too far west along the equator (Figs. 3-4; AchutaRao and Sperber 2006; Joseph and Nigam 2006). MPI_ECHAM5 has stronger correlations than observed. On the regional scale, negative correlations in the western Indian Ocean and positive correlations in the eastern equatorial Indian Ocean in GFDL_CM_2.0, MPI and MRI are stronger than observed. These regional signals are weak in the long term mean of the observations, and they exhibit a pronounced decadal modulation. For example, they are strong during the period 1976-2000 and weak during 1951-75 (Annamalai and Liu 2005).

Another diagnostic employed to verify the effect of ENSO on the precipitation variability over continental India is the regression of Nino3.4 SST anomalies on to precipitation anomalies (Fig. 10). To be consistent with correlation diagnostics, the regression is calculated separately for each realization, and then an ensemble-mean pattern is computed. In agreement with observations, except in NCAR_PCM, the effect of ENSO on the model rainfall variability is felt over the entire Indian subcontinent. Despite a reasonable simulation of mean monsoon precipitation climatology, HadCM3 does not simulate well the ENSO-monsoon relationship (shown later in Fig. 15a). Further, the teleconnection is not robust among the ensemble members in HadCM3. Turner et al. (2005) documented similar difficulties in their analysis of HadCM3 integrations. NCAR_PCM also does not simulate well the monsoon-ENSO relationship. As seen in Figs. 1-4, it had the least realistic rainfall climatology over India and the temporal evolution of SST and precipitation anomalies along the equatorial Pacific was poorly represented. In addition, during El Niño events warm SST signals are confined to equatorial west Pacific, and combined with weak descent anomalies, negative precipitation anomalies over the Maritime Continent are not simulated in both NCAR_PCM and HadCM3. Thus, the required teleconnection mechanism is not present in these models. Henceforth these two models are not analyzed any further. We return to this issue in Section 5d.

Figure 11 shows the monsoon-ENSO correlation patterns obtained from the 1pctto2x runs. For this global warming experiment the MPI_ECHAM5 has three realizations, while the remaining models have only one realization. In contrast to the results of Ashrit et al. (2005), we find that in all four models the basic monsoon-ENSO relationship remains intact under this climate change scenario. Compared to 20c3m runs, in the 1pctto2x integrations the temporal evolution of Nino3.4 SST anomalies remain similar (Fig. 2b). In the two GFDL models and in the MRI model the mon-

soon-ENSO teleconnection in the Pacific actually strengthens in the global warming run, while in MPI_ECHAM5 it weakens slightly compared to the 20c3m runs (Fig. 9). In all four models, the positive correlations, particularly near Java-Sumatra in the eastern equatorial Indian Ocean have increased in the 1pctto2x runs.

(b) Lead/lag relationship between ENSO and monsoon

To check if the models represent the timing of the teleconnection correctly, lead/lag correlations between Nino3.4 (5^{o}S-5^{o}N, 120^{o}W- 170^{o}W) SST anomalies and AIR anomalies are computed. The Nino3.4 domain is chosen since in observations the strongest anticorrelations between AIR and SST occur over this region (Fig. 9a). For each of the four models, this correlation is calculated separately for each of realization, and then an ensemble-mean pattern is computed.

In observations negative correlations (Fig. 12a, black line) occur only after April, The observed maximum correlation after the monsoon season has led to suggestions that variations in the intensity of the monsoon can potentially influence the surface wind-stress in the equatorial Pacific and thereby modify the statistical properties of ENSO (e.g., Kirtman and Shukla 2000; Wu and Kirtman 2004). In the 20c3m simulations, all the models capture the inverse relationship during boreal summer but the maximum negative correlation occurs too early in the GFDL_CM_2.0, MRI, and MPI_ECHAM5 simulations. While three of the models reasonably represent the spring predictability barrier, seen as the near zero correlations during the preceding winter/spring, the MPI_ECHAM5 simulations (violet line, Fig. 12a) are incorrect in this respect, with the presence of pronounced negative correlations from the preceding winter. Of the four models, GFDL_CM_2.1 model best captures the timing in the relationship correctly. The ability to resolve the timing is possibly related to the ability in simulating the space-time evolution of SST and the

associated diabatic heating anomalies during El Niño events (Section 2b). In the 1pctto2x integrations (Fig. 12b) the tendency is for the spring predictability barrier to be more apparent, and in the case of GFDL_CM_2.0 and MRI there is a tendency for the negative correlations to persist for about 3-6 months after the monsoon season. Overall, the results presented so far indicate that the ENSO-monsoon relationship remains strong and stable in a warmer climate.

(c) Decadal modulation of the ENSO-monsoon relationship

Figure 13 shows the 21-year sliding correlation between AIR and NINO3.4 SST indices, and for all the realizations. For comparison, the observed result is repeated in all the panels. As in observations, the simulated ENSO-monsoon relationship waxes and wanes at decadal-interdecadal time scales, implying that ENSO-monsoon forecast skill is not robust over the entire period. For the GFDL_CM_2.0, GFDL_CM_2.1 and MRI models the overall range and timescales of variation of the correlation coefficients are similar to that observed. By contrast all three realizations of the MPI_ECHAM5 model yield a correlation coefficient that is somewhat more stable in time than that actually observed. For each model, the curves in Fig. 13 are not coherent in time among the individual realizations. Given that the 20c3m runs include temporal variations of climate forcing, the simulations could in principle exhibit a systematic trend in the correlation, but there is no evidence for a systematic change in the latter portion of the 20th century. Our model results suggest that the observed weakening of the monsoon-ENSO relationship is due to interdecadal vacillations of this teleconnection, rather than to global warming as suggested by Krishnakumar et al. (1999). It is possible that the behavior in the 1990s, could be attributed to stronger El Niños and the associated regional SST anomalies (Annamalai and Liu 2005).

The decadal and interdecadal modulations of the AIR-NINO3.4 SST correlation are also apparent in the 1pctto2x simulations (Fig. 14). Indeed the overall behavior of the correlations for each model is similar to that seen in its 20c3m runs (Fig. 13). So we find little evidence for a strong effect of global warming on the ENSO-monsoon relationship. Contrary to the modeling results of Ashrit et al. (2005), the results presented here do not suggest that there will be a a sudden breakdown in the ENSO-monsoon relationship over the next century. Additionally, at decadal time scales the diversity in the phasing among the ensemble members (Figs. 13-14) suggests an inherent difficulty in predicting the breakdown in the ENSO-monsoon relationship. The possible reasons for the decadal modulation in the ENSO-monsoon association will be reported in a future study.

(d) Role of the basic state in the ENSO-monsoon relationship

Finally we revisit the issue of ENSO-monsoon teleconnection in some of the IPCC AR4 models that have either poor mean monsoon precipitation climatology and/or unrealistic representation of basic ENSO behavior. Figure 15 shows the lagged correlations between AIR and Nino3.4 SST, indicating that none of these models reproduces the observed correlation pattern. For example, the correlations in GISS_EH (blue line) are unrealistically small everywhere while the correlation is much too strong along the entire equatorial Pacific in the FGOALS-g1.0 (IAP: green line) model. On the other hand, positive correlations prevail throughout in MIRO_HIGH model. Over the Nino3.4 region, the standard deviation of monthly anomalies of SST in FGOALS-g1.0 is 150% stronger than those in the HadISST observations (AchutaRao and Sperber 2006) indicating unrealistic ENSO variability. In GISS_EH, the ENSO variability is weak and lacks spatial coherence (Fig. 1 in Joseph and Nigam 2006), and also the mean monsoon precipita-

tion and its interannual variability over India (not shown) are both too weak compared to observations. These aspects in GISS_EH may account for weaker correlations. In HadCM3, significant negative correlations start about one year before the monsoon season, consistent with the results presented in Turner et al. (2005). Despite some improvements in the timing and spatial correlations in HadGEM1 compared to its earlier version HadCM3, the strength of mean monsoon precipitation over Indian subcontinent is less than 2.0 mm/day (not shown). Finally, the strongest negative correlation in PCM is noted in May-June (yellow line) during which ENSO variability peaks (Fig. 2a). In summary, in agreement with others, our diagnostics reveal that a proper representation of the basic state is a pre-requisite to capture the natural modes of variability, and their linkages.

6. Summary and Conclusions

The availability of the extensive integrations produced for the IPCC AR4 intercomparison affords an opportunity to study the performance of current global climate models and assess the implications for forecasts of future climate. Here we have concentrated on assessing the variability of South Asia summer monsoon rainfall and ENSO characteristics. ENSO provides the most systematic forcing of interannual monsoon variability and so we have focussed on the relationship between ENSO and the monsoon. Models that adequately reproduce the observed spatial, seasonal and decadal aspects of the ENSO-monsoon connection under present day conditions may have a degree of credibility in forecasting monsoon response to expected climate forcing.

We found that there is a very wide variation in the quality of the simulation of the mean monsoon and its variability among the AR4 models. We examined the mean precipitation climatology over South Asian and over the broader ASM region in the 20th century retrospective runs

produced by 18 models. We judged only six of these models could be considered to have realistic rainfall results as shown by high pattern correlation and low root mean square differences relative to observations. This judgement is consistent with Sperber (1999) who found that models that have realistic ENSO-monsoon association have high pattern correlation with observations in the vicinity of India. For these six models and for the 20c3m simulations, an assessment of SST and precipitation anomalies along the equatorial Pacific during El Niño events depict considerable differences when compared with observations. For these 6 models, we calculated the contemporaneous correlation of SST in the Indo-Pacific region with the AIR index. Four models exhibit a robust teleconnection pattern that is reasonably close to that observed. We then computed lagged correlations between the AIR index and Nino3.4 SST of these four models. All the models capture the inverse relationship during boreal summer, but the timing of the maximum magnitude of correlation is correctly reproduced only by the GFDL_CM_2.1. In the other 3 models the maximum correlation occurs too early. Overall we find that the models that best capture the ENSO-monsoon teleconnection are those that correctly simulate the timing and location of SST and diabatic heating anomalies in the equatorial Pacific, and the resultant anomalous Walker Circulation with considerable descent anomalies over India during El Niño events.

The 20th century integrations are long enough to characterize the evolution of the ENSO-monsoon correlations over decadal-to-interdecadal timescales. When examined in this way all the models reveal a waxing and waning in the ENSO-monsoon relationship at decadal-to-interdecadal time scales. The overall behavior in this respect is similar to that seen in the observed 20th century record, but there is no apparent agreement in the phases of these fluctuations among the model realizations. Given that the 20c3m runs include the evolving climate forcing over the 20th century, the simulations could, in principle, show a systematic trend in the ENSO-monsoon corre-

lation in response to the changing forcing, but it is hard to see evidence for this (Fig. 13). Thus these model results do not support the contention of Krishnakumar et al. (1999) that the recent apparent weakening of the monsoon-El Niño connection can be attributed to global warming. Rather than a response to global climate change the variations in strength of the ENSO-monsoon correlation would appear to be spontaneous. One intriguing idea is that ENSO teleconnections may be non-linear, and so if the strength of ENSO in a simulation has a systematic interdecadal variation, then the ENSO-monsoon relation would appear to have its own long period variation.

The analysis was repeated for each of the four models using results from integrations in which the atmospheric CO_2 concentration was raised to twice pre-industrial values. For each model there are increases in both the mean monsoon rainfall over the Indian sub-continent (by 5-25%) and in its interannual variability (5-10%) compared to the 20c3m runs. We find for each model that the ENSO-monsoon correlation, including the overall behavior of the decadal-interdecadal modulation, in the global warming runs is very similar to that in the 20^{th} century runs. We find no support for the suggestion advanced by earlier investigators (e.g, Ashrit et al. 2005) that the ENSO-monsoon connection could weaken as global climate warms. This result, though plausible, needs to be taken with some caution because of the diversity in the simulation of ENSO variability in the coupled models we have analyzed. To reiterate, we need to re-visit this important issue when the simulated ENSO variability improves in coupled models. On the other hand, observed weakened ENSO-monsoon relationship around 1920s (Fig. 13a) is not necessarily due to global warming.

In summary, consistent with others (e.g, Turner et al. 2005), our diagnostics indicate that a proper representation of the basic state is a pre-requisite to capture the natural modes of climate variability. The results based on these model integrations indicate that the natural modes of vari-

abilities and their linkages in the tropical climate system will remain intact in the global warming situations. A direct implication is that the component of the seasonal mean rainfall over India forced by ENSO appears to be predictable in the future warming scenario.

Our future investigations will focus on the possible reasons for the increase in the mean and variability of the monsoon rainfall in the climate change experiments, and the factors responsible for the decadal modulation of the ENSO-monsoon relationship. Additionally, the possible reasons for stronger ENSO-monsoon relationship in warming experiments will be addressed.

Acknowledgments. The authors thank Prof. Sumant Nigam, the Editor, and the anonymous reviewers for their comments that improved the manuscript. This research was partly funded by the NOAA Climate Program Office and the Office of Global Programs as a Climate Model Evaluation Project (CMEP) under the U.S. CLIVAR Program http://www.usclivar.org/index.html and partly by the Japan Agency for Marine Earth Science and Technology (JAMSTEC) through its sponsorship of the International Pacific Research Center. We acknowledge the international modeling groups for providing their data for analysis, the Program for Climate Model Diagnosis and Intercomparison (PCMDI) for collecting and archiving the model data, the JSC/CLIVAR Working Group on Coupled Modelling (WGCM) and their Coupled Model Intercomparison Project (CMIP) and Climate Simulation Panel for organizing the model data analysis activity, and the IPCC WG1 TSU for technical support. The IPCC Data Archive at Lawrence Livermore National Laboratory is supported by the Office of Science, U.S. Department of Energy. K. R. Sperber was supported under the auspices of the U.S. Department of Energy Office of Science, Climate Change Prediction Program by University of California Lawrence Livermore National Laboratory under contract No. W-7405-Eng-48.

References

AchutaRao, K., and K. R. Sperber, 2002: Simulation of the El Niño Southern Oscillation: Results from the coupled model intercomparison project. *Climate Dyn.*, **19**: 191-209.

----------, and ----------, 2006: ENSO simulation in coupled ocean-atmosphere models: Are the current models better? *Climate Dyn.* **27**: 1-15 (DOI 10.1007/s00382-006-0119-7)

Annamalai, H., J.M. Slingo, K.R. Sperber and K. Hodges, 1999: The mean evolution and variability of the Asian summer monsoon: comparison of ECMWF and NCEP/NCAR reanalyses. *Mon. Wea. Rev.,* **127,** 1157-1186.

--------, and P. Liu, 2005: Response of the Asian Summer Monsoon to changes in El Niño properties. *Quart. J. Roy. Meteor. Soc.,* **131,** 805-831.

--------, and K.R. Sperber, 2005: Regional heat sources and the active and break phases of boreal summer intraseasonal (30-50 day) variability. *J. Atmos. Sci.,* **62,** 2726-2748.

Ashrit, R.G., K. Rupakumar, and K. Krishnakumar, 2001: ENSO-monsoon relationships in a greenhouse warming scenario. *Geophys. Res. Lett.,* **28,** 1727-1730.

--------, H. Douville, and K. Rupakumar, 2003: Response of Indian monsoon and ENSO-monsoon teleconnection to enhanced greenhouse effect in the CNRM coupled model. *J. Meteor. Soc. Japan,* **81,** 779-803.

--------, A. Kitoh, and S. Yukimoto, 2005: Transient response of ENSO-monsoon teleconnection in MRI-CGCM2.2 climate change simulations. *J. Meteor. Soc. Japan* (in press).

Charney, J.G., and J. Shukla, 1981: Predictability of monsoons. Monsoon Dynamics, Cambridge University Press, New York, USA, pp 99-109.

Fennessy, M., J.L. Kinter III, B. Kirtman, L. Marx, S. Nigam, E. Schneider, J. Shukla, D. Straus, A. Vernekar, Y. Xue, and J. Zhou, 1994: The simulated Indian monsoon: a GCM sensitivity study. *J. Clim.,* **7,** 33-43.

Guilyardi, E., 2006: El Niño-mean state-seasonal cycle interactions in a multi-model ensemble. *Climate. Dyn*. 26, 329-348 (DOI 10.1007/s00382-005-0084-6)

Hu, Z.Z., M. Latif, E. Roeckner, and L. Bengtsson, 2000: Intensified Asian summer monsoon and its variability in a coupled model forced by increasing greenhouse gas concentrations. *Geophys. Res. Lett.,* **27,** 2681-2684.

Joseph, R., and S. Nigam, 2006: ENSO evolution and teleconnection in IPCC's 20th century climate simulations: Realistic representation?

Ju, J., and J.M. Slingo, 1995: The Asian summer monsoon and ENSO. *Quart. J. Roy. Meteor. Soc.,* **121,** 1133-1168.

Kinter, J.L., K. Miyakoda, and S. Yang, 2002: Recent changes in the connection from the Asian monsoon to ENSO. *J. Climate,* **15,** 1203-1214.

Kirtman, B.P., and J. Shukla, 2000: Influence of the Indian summer monsoon on ENSO. *Quart. J. Roy. Meteor. Soc*., **126,** 1623-1646.

Knutson, T.R., and S. Manabe 1994: Impact of increased CO2 on simulated ENSO-like phenomena. *Geophys. Res. Lett.,* **21,** 2295-2298.

Krishnakumar, K., B. Rajagopalan, and M.A. Cane, 1999: On the weakening relationship between the Indian monsoon and ENSO. *Science,* **284,** 2156-2159.

Latif, M and co-authors, 1998: A review of the predictability and prediction of ENSO. *J. Geophys. Res.*, **103,** 14, 375-14, 393.

Latif, M., and co-authors, 2001: ENSIP: the El Niño simulation intercomparison project. *Climate Dyn,* **18,** 255-276.

Lau, N.C., and M.J. Nath, 2000: Impact of ENSO on the variability of the Asian-Australian monsoon as simulated in GCM experiments. *J. Climate,* **13,** 4287-4309.

Mahfouf, J.F., D. Cariolle, J.F. Royer, J.F. Geleyn, and B. Timbal, 1994: Response of the Meteo-France climate model to changes in CO_2 and sea surface temperature. *Climate. Dyn.,* **9,** 345-362.

May, W., 2002: Simulated changes of the Indian summer monsoon under enhanced greenhouse gas conditions in a global time-slice experiment. *Geophys. Res. Lett.,* **29,** 10.1029/ 2001GL013808.

Meehl, G.A., and W.M. Washington, 1993: South Asian summer monsoon variability in a model with doubled atmospheric carbon dioxide concentration. *Science,* **260,** 1101-1104.

--------., P. Gent, J.M. Arblaster, B. Otto-Bliesner, E. Brady, and A. Craig, 2001: Factors that affect amplitude of El Niño in global coupled climate models. *Climate Dyn,* **17,** 515-526.

---------, and J.M. Arblaster, 2002: Indian monsoon GCM sensitivity experiments testing tropospheric biennial oscillation transition conditions. *J. Climate,* **15,** 923-944.

---------, and J.M. Arblaster 2003: Mechanisms for projected future changes in south Asian monsoon precipitation. *Climate Dyn,* **21,** 659-675.

Nigam, S., 1994: On the dynamical basis for the Asian summer monsoon rainfall-El Nino relationship. *J. Climate,* **7,** 1750-1771.

Parthasarathy, B., K. Rupakumar and A.A. Munot, 1991: Evidence of secular variations in Indian monsoon rainfall-circulation relationships. *J. Climate,* **4,** 927-938.

Parthasarathy, B., A.A. Munot and D.R. Kothawale, 1994: All-India monthly and seasonal rainfall series: 1871-1993. *Theor. Appl. Climatol.,* **49,** 217-224.

Rajeevan, M., J. Bhate, J.D. Kale, and B. Lal., 2005: Development of a high resolution daily-gridded rainfall data for the Indian region. Met. Monograph Climatology No. 22/2005, India Metorological Department, Pune, India.

Rasmusson, E.M., and T.H. Carpenter, 1983: The relationship between eastern equatorial Pacific sea surface temperature and surface wind fields associated with the Southern Oscillation/El Niño. *Mon. Wea. Rev.,* **111,** 517-528.

Rayner, N. A., D. E. Parker, E. B. Horton, C. K. Folland, L. V. Alexander, D. P. Rowell, E. C. Kent, and A. Kaplan, 2003: Global analyses of sea surface temperature, sea ice, and night marine air temperature since the late nineteenth century. *J. Geophys. Res.,* **108,** D14, 4407, doi:10.1029/2002JD002670.

Sikka, D.R., 1980: Some aspects of the large-scale fluctuations of summer monsoon rainfall over India in relation to fluctuations in the planetary and regional scale circulation parameters. *Proc. Indian Natl. Acad. Sci.,* **89,** 179-195.

Shukla, J., 1984: Predictability of Time averages: Part II. The influence of the boundary forcing, in D.M. Burridge and E. Kallen, Eds., Problems and Prospects in Long and Medium range weather forecasting, Springer-Verlag, London, pp 155-206.

--------, and D.A. Paolino, 1983: The southern oscillation and long range forecasting of the summer monsoon rainfall over India. *Mon. Wea. Rev.,* **111,** 1830-1837.

--------, 1995: Predictability of the tropical atmosphere, the tropical ocean and TOGA'. Proceedings of the international conference on the Tropical Ocean and Global Atmosphere (TOGA) programme. WCRP-91. World Climate Research Program, Geneva, Switzerland.

Slingo, J.M., and H. Annamalai, 2000: 1997: The El Niño of the century and the response of the Indian summer monsoon. *Mon. Wea. Rev.,* **128,** 1778-1797.

Soman, M.K., and J.M. Slingo, 1997: Sensitivity of the Asian summer monsoon to aspects of sea surface temperature anomalies in the tropical Pacific Ocean. *Quart. J. Roy. Meteor. Soc.,* **123,** 309-336.

Sperber, K.R.,and T.N. Palmer, 1996: Interannual tropical rainfall variability in general circulation model simulations associated with the Atmospheric Model Intercomparison Project. *J. Climate,* **9,** 2727-2750.

Sperber, K.R., 1999: Are revised models better models? A skill score assessment of regional interannual variability. *Geophys. Res. Lett.,* **26,** 1267-1270.

Timbal, B., J.F. Mahfouf, J.F. Royer, and D. Cariollle, 1995: Sensitivity to prescribed changes in sea surface temperature and sea-ice in doubled carbon dioxide experiments. *Climate. Dyn.,* **12,** 1-20.

Turner, A.G., P.M. Inness, and J.M. Slingo, 2005: The role of the basic state in the ENSO-monsoon relationship and implications for predictability. *Quart. J. Roy. Meteor. Soc.,* **131,** 781-804.

Walker, G.T., and E.W. Bliss, 1932: World Weather V. *Mem. R. Meteor. Soc.,* **4,** 53-84.

Wang, B., R. Wu, and K.M. Lau, 2001: Interannual variability of the Asian summer monsoon: Contrast between the Indian and western north Pacific-East Asian monsoons. *J. Climate,* **14,** 4073-4090.

Webster, P.J., V.O. Magana, T.N. Palmer, J. Shukla, R.A. Thomas, M. Yanai, and T. Yasunari, 1998: The monsoon: Processes, predictability and prediction. *J. Geophys. Res.,* **103,** 14451-14510.

Wu, R., and B.P. Kirtman, 2003: On the impacts of Indian summer monsoon on ENSO in a coupled GCM. *Quart. J. Roy. Meteor. Soc*., **129,** 3439-3468.

Xie, P., and P. Arkin, 1996: Analyses of global monthly precipitation using gauge observations, satellite estimates, and numerical model predictions. *J. Climate,* **9,** 840-858.

Yukimoto, S., A. Noda, T. Uchiyama, and S. Kusunoki, 2005: Climate change of the twentieth through twenty-first centuries simulated by MRI-CGCM2.3. *Papers in Meteor. Geophys* (submitted).

FIGURE CAPTIONS

Figure 1: Seasonal mean (June-September) precipitation climatology (*mm/day*, shaded) and standard deviation (in dashed contours with an interval of 1.0 *mm/day*) from the 20c3m integrations of (a) GFDL_CM2.0; (b) GFDL_CM2.1, (c) MPI_ECHAM5, (d) MRI, (e) HadCM3, and (f) NCAR_PCM. Observations are shown in (g). The pattern correlation and the root-mean-square difference (RMSD) between the model and CMAP observations over the Asian Summer Monsoon region (40-180^{o}E, 25^{o}S-40^{o}N), and over the Indian monsoon region (7-30^{o}N, 65-95^{o}E) are given in parenthesis, respectively; (h) annual cycle of precipitation (*mm/day*) over the south Asian monsoon region (60-100^{o}E, 10-25^{o}N).

Figure 2: Monthly temporal evolution of composite SST anomalies (in standard deviations) averaged over the NINO3.4 region (5^{o}S-5^{o}N, 120-170^{o}W) from different coupled models: (a) 20c3m and (b) 1pctto2x simulations. The composites are based on strong El Nino events (> 1.0 std of SST anomalies over the NINO3.4 region). The corresponding figure from observations is also shown in (a). Years 0 and 1 correspond to the typical life cycle of El Nino in which it peaks around December at the end of Year 0.

Figure 3: Monthly SST evolution in the equatorial (5^{o}S-5^{o}N) Pacific during El Nino years: (a) Observations, (ii) NCAR_PCM, and (c) GFDL_CM_2.1. Horizontal dotted lines represent the duration of the summer monsoon season. The time co-ordinate starts with January of Year (0) of the developing phase of El Nino and ends with December of Year (1) of the decaying phase of El Nino. The composites are based on strong El Nino events (> 1.0 std of SST anomalies over the NINO3.4 region during June-September).

Figure 4: Same as Fig. 3 but for precipitation anomalies: (a) Observations, (b) NCAR_PCM, and (c) GFDL_CM_2.1. Positive values are shaded progressively while negative values are shown in contour with an interval of 2.0 *mm/day*.

Figure 5: Same as Fig. 3 but for anomalous Velocity Potential at 200hPa (m^2 s^{-1}): (a) NCEP_NCAR reanalysis, (b) NCAR_PCM, and (c) GFDL_CM_2.1

Figure 6: Surface temperature difference (^{o}C; June-September) between the 1pctto2x and 20c3m integrations: (a) GFDL_CM_2.0, (b) GFDL_CM_2.1, (c) HadCM3, (d) NCAR_PCM, (e) MPI_ECHAM5, and (f) MRI. The shading interval is different for the last panels. Only values greater 99% significance level is shown.

Figure 7: Difference in precipitation (shaded) and standard deviations in precipitation (contours) between 1pctto2x and 20c3m integrations (June-September): (a) GFDL_CM_2.0, (b) GFDL_CM_2.1, (c) MPI_ECHAM5, (d) MRI, (e) HadCM3 and (f) NCAR_PCM. The contour interval is (0.5 mm/day). Values are significant at 90% level (except for MRI in which the values are significant at 95% level).

Figure 8: Temporal evolution of pentad mean precipitation averaged over the south Asian monsoon region (60^{o}E-100^{o}E, 5^{o}N-25^{o}N) for: (a) GFDL_CM_2.0 and (b) MRI. The annual cycle is based on

the 40-year climatology (1961-2000 for control) and various sub-periods for the SRESA1B experiments, and also from the 1pctto2x integrations. For comparison, the mean annual cycle constructed from three different observed products are also shown. The pentads between the vertical lines correspond to the monsoon season (June-September).

Figure 9: Correlation patterns between seasonal mean (June – September) between AIR indices and sea surface temperature (SST) anomalies from the 20c3m simulations: (a) Observations, (b) GFDL_CM_2.0, (c) MPI_ECHAM5, (d) GFDL_CM_2.1, (e) MRI, and (f) NCAR_PCM. Values significant at greater than 95% level are only shown. Negative (positive) values are shaded progressively (shown as contour with an interval of 0.08).

Figure 10: Regression patterns between seasonal mean (June – September) NINO3.4 SST indices and precipitation anomalies (*mm/day*) from the 20c3m simulations: (a) Observations, (b) GFDL_CM_2.0, (c) GFDL_CM_2.1, (d) MPI_ECHAM5, (e) MRI, and (f) NCAR_PCM. Values significant at greater than 95% level are only shown. Negative (positive) values are shaded progressively (shown as contour with an interval of 0.2). All regressions have been scaled by a one standard deviation perturbation of NINO3.4 SST.

Figure 11: Same as Fig. 7 but for 1pctto2x integrations.

Figure 12: Lag/lead correlation between AIR anomalies and NINO3.4 SST anomalies: (a) 20c3m, and (b) 1pctto2x simulations. In both panels, the results from observations are also shown. Horizontal dotted lines represent the 5% significance level. Lag –12 corresponds to NINO3.4 SST anomalies one year before the monsoon season.

Figure 13: Shown are 21-year sliding correlations between all-India rainfall (AIR) and NINO3.4 SST anomalies (JJAS) for the individual realizations: (a) GFDL_CM_2.0, (b) GFDL_CM_2.1, (c) MPI_ECHAM5, (d) MRI. In all the panels, results from observation are also shown. The horizontal line shows the 5% significance level.

Figure 14: Same as Fig. 11 but from the 1pctto2x runs: (a) single realization from the three models, and (b) three realizations from MPI_ECHAM5. The horizontal lines represent the 5% significance level.

Figure 15: Same as Fig. 12a but for models that have either poor monsoon precipitation climatology and/or unrealistic representation of ENSO variability. Horizontal dotted line represents the 5% significance level. Lag –12 corresponds to Nino3.4 SST anomalies one year before the monsoon season.

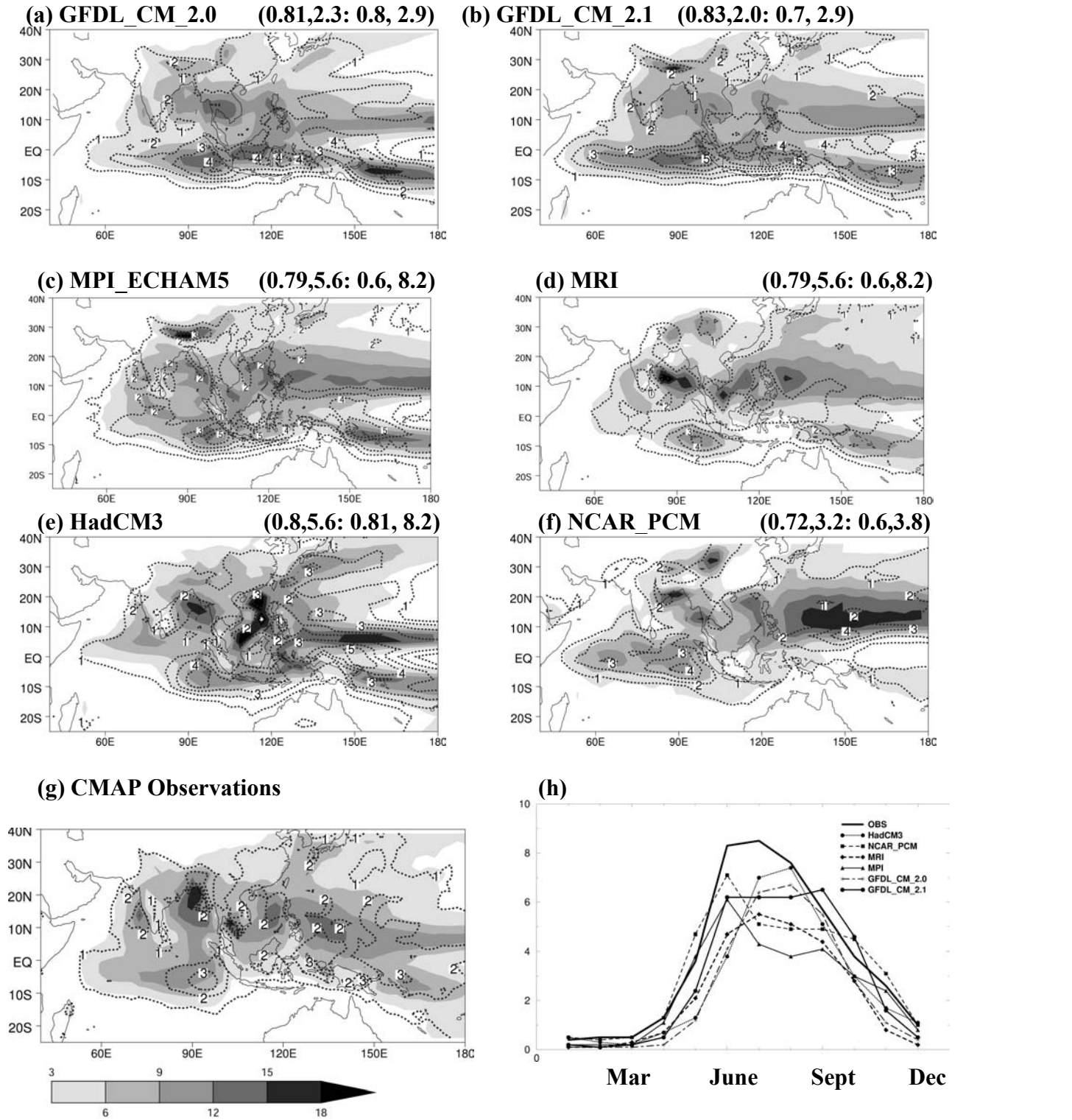

Figure 1: Seasonal mean (June-September) precipitation climatology (*mm/day*, shaded) and standard deviation (in dashed contours with an interval of 1.0 *mm/day*) from the 20c3m integrations of (a) GFDL_CM2.0; (b) GFDL_CM2.1, (c) MPI_ECHAM5, (d) MRI, (e) HadCM3, and (f) NCAR_PCM. Observations are shown in (g). The pattern correlation and the root-mean-square difference (RMSD) between the model and CMAP observations over the Asian Summer Monsoon region (40-180^{o}E, 25^{o}S-40^{o}N), and over the Indian monsoon region (7-30^{o}N, 65-95^{o}E) are given in parenthesis, respectively; (h) annual cycle of precipitation (*mm/day*) over the south Asian monsoon region (60-100^{o}E, 10-25^{o}N).

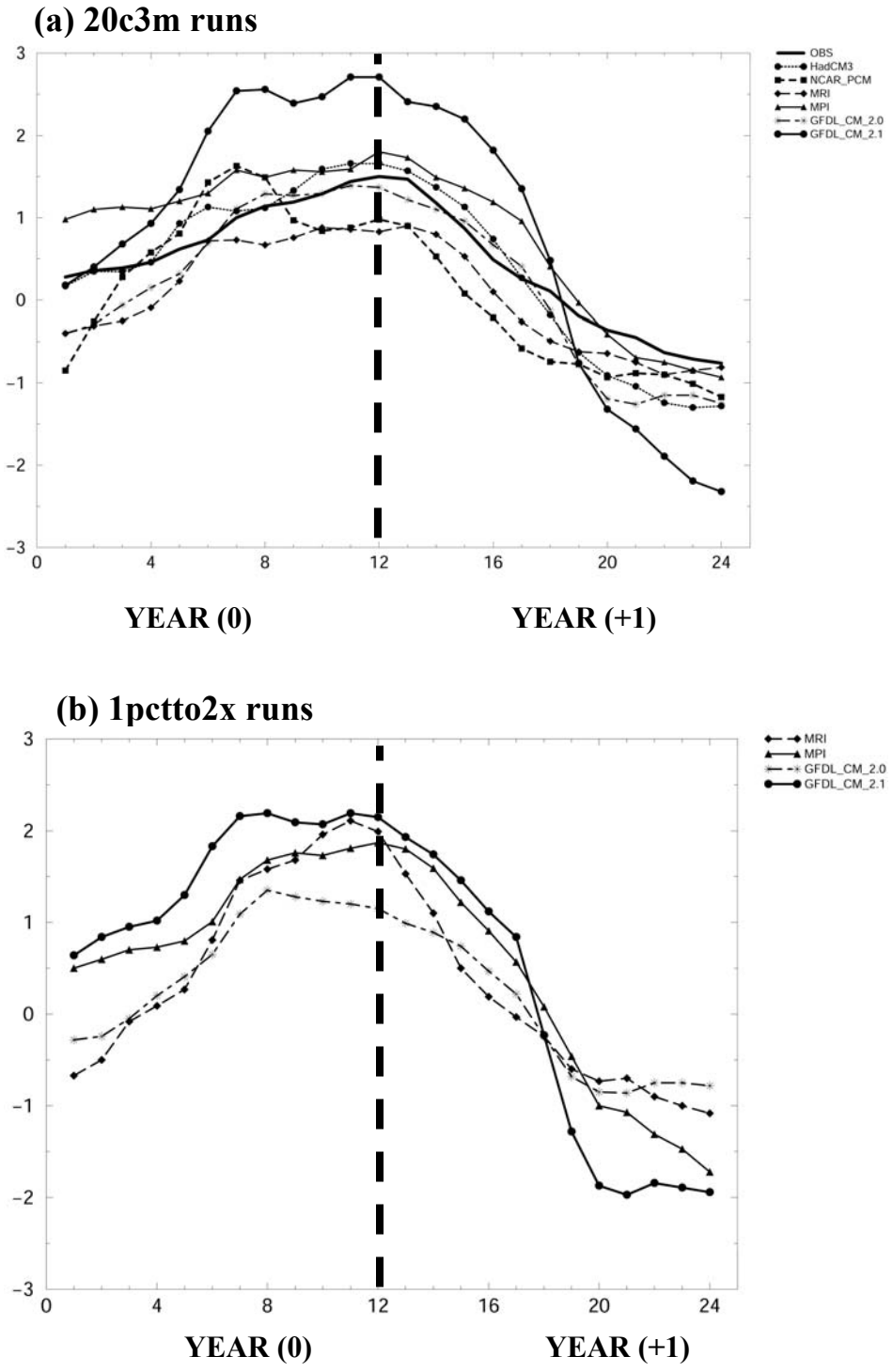

Figure 2: Monthly temporal evolution of composite SST anomalies (in standard deviations) averaged over the NINO3.4 region (5°S-5°N, 120-170°W) from different coupled models: (a) 20c3m and (b) 1pctto2x simulations. The composites are based on strong El Nino events (> 1.0 std of SST anomalies over the NINO3.4 region). The corresponding figure from observations is also shown in (a). Years 0 and 1 correspond to the typical life cycle of El Nino in which it peaks around December at the end of Year 0.

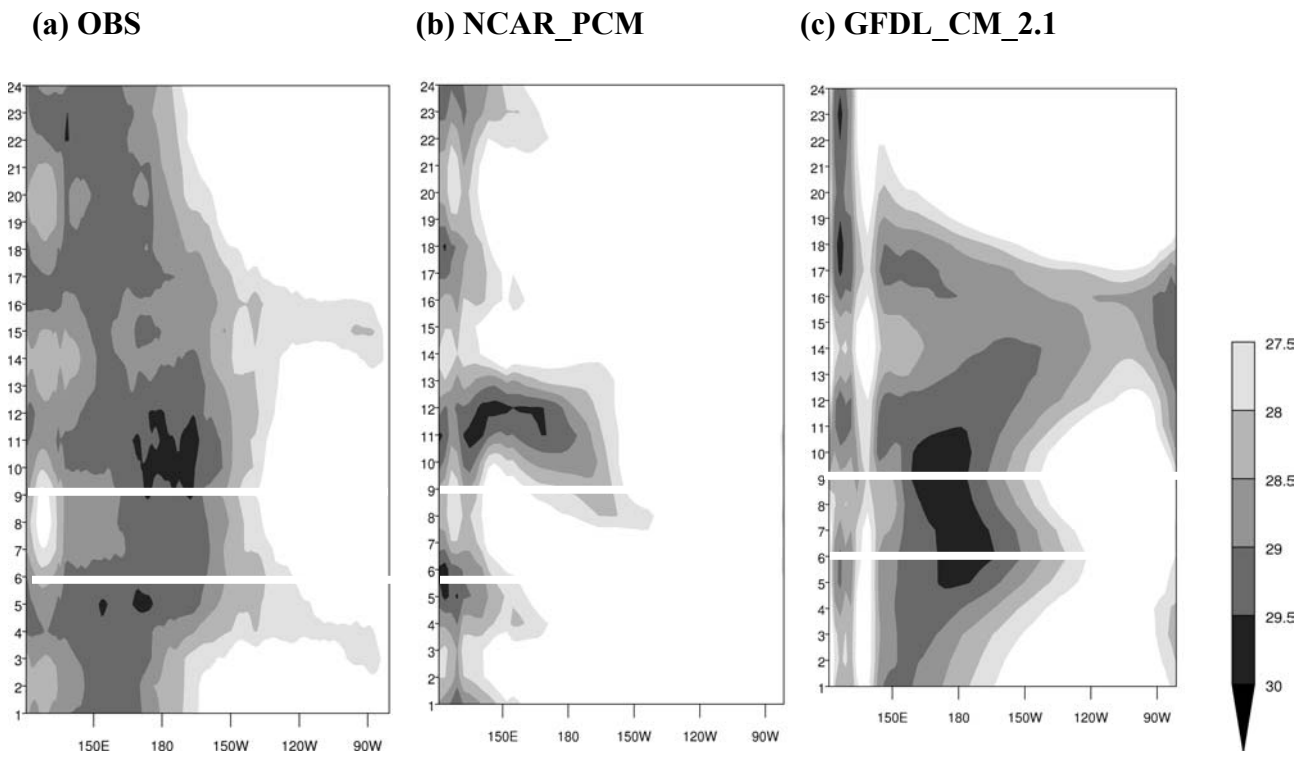

Figure 3: Monthly SST evolution in the equatorial (5°S-5°N) Pacific during El Nino years: (a) Observations, (ii) NCAR_PCM, and (c) GFDL_CM_2.1. Horizontal dotted lines represent the duration of the summer monsoon season. The time co-ordinate starts with January of Year (0) of the developing phase of El Nino and ends with December of Year (1) of the decaying phase of El Nino. The composites are based on strong El Nino events (> 1.0 std of SST anomalies over the NINO3.4 region during June-September).

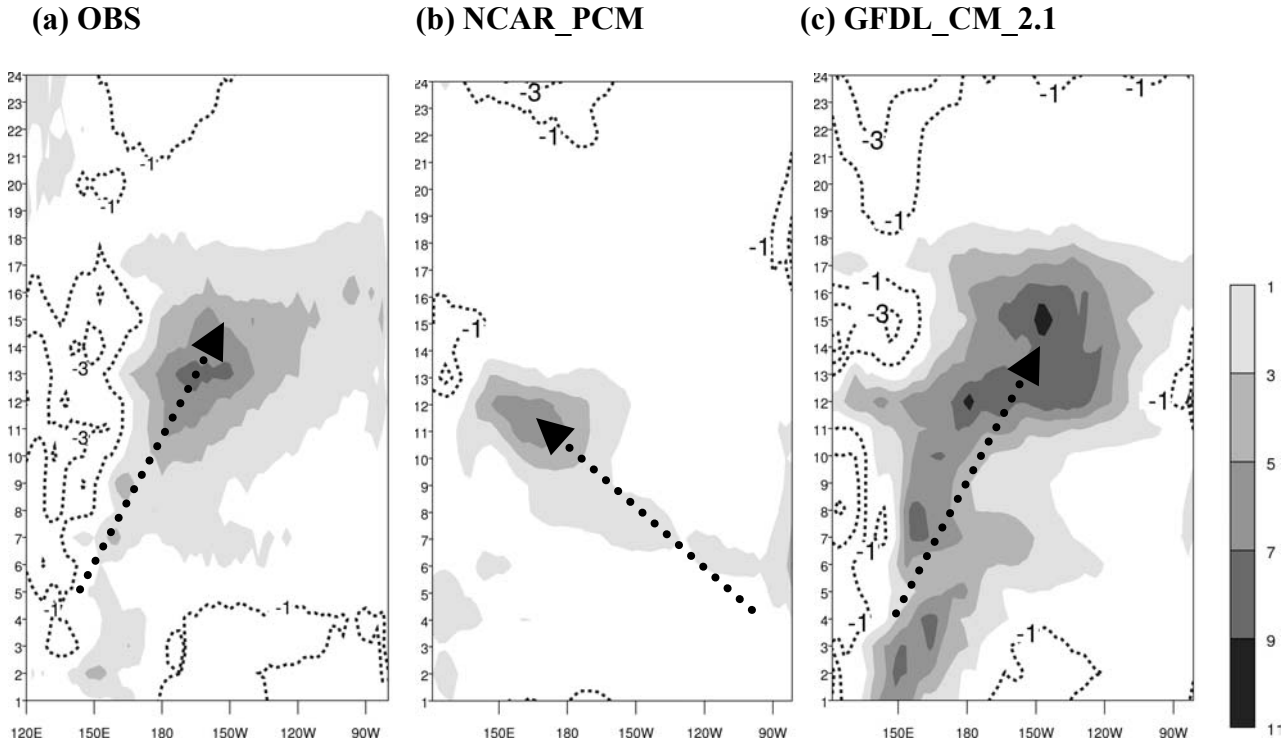

Figure 4: Same as Fig. 3 but for precipitation anomalies: (a) Observations, (b) NCAR_PCM, and (c) GFDL_CM_2.1. Positive values are shaded progressively while negative values are shown in contour with an interval of 2.0 *mm/day*.

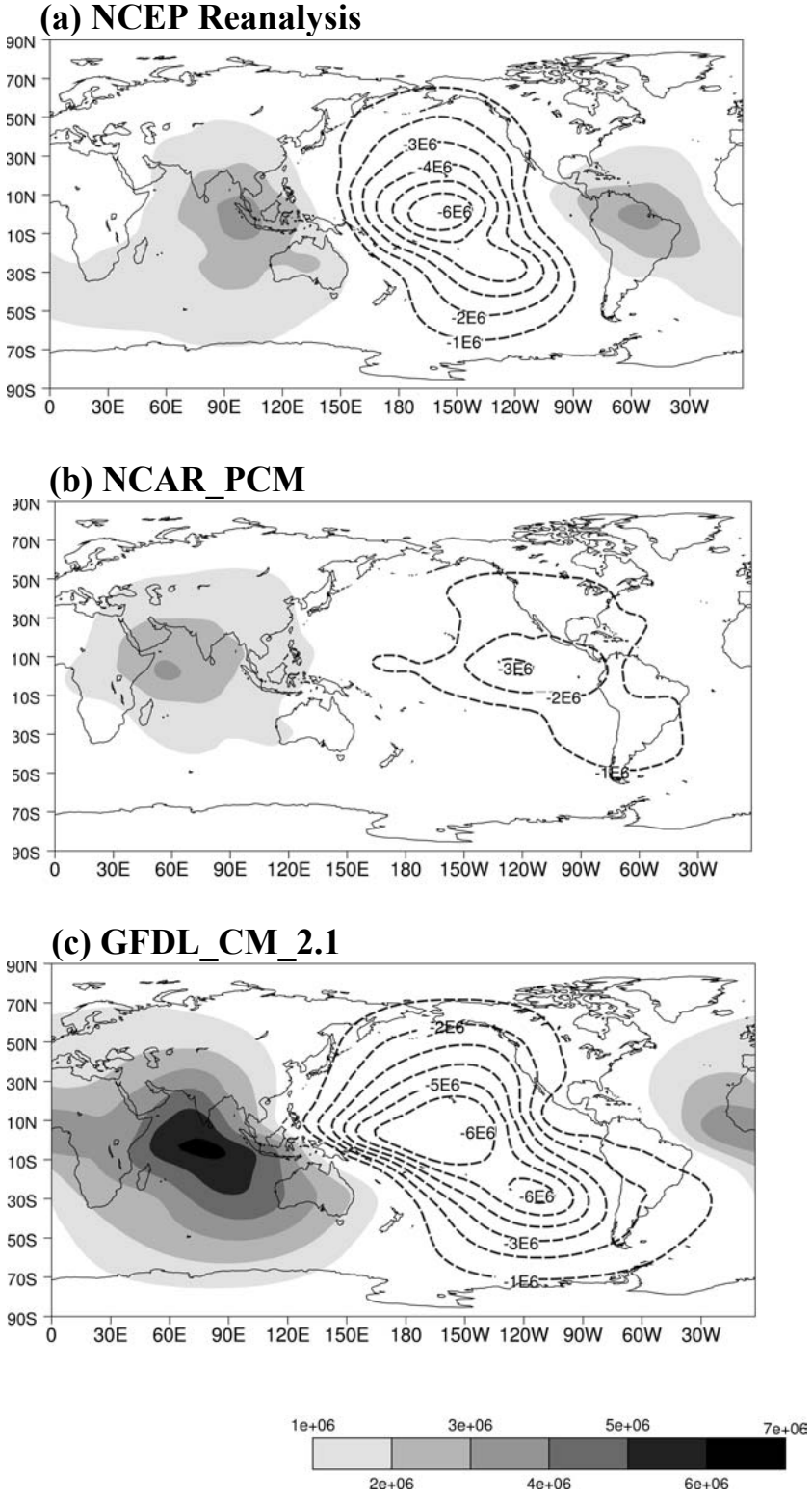

Figure 5: Same as Fig. 3 but for anomalous Velocity Potential at 200hPa (m^2 s^{-1}): (a) NCEP_NCAR reanalysis, (b) NCAR_PCM, and (c) GFDL_CM_2.1

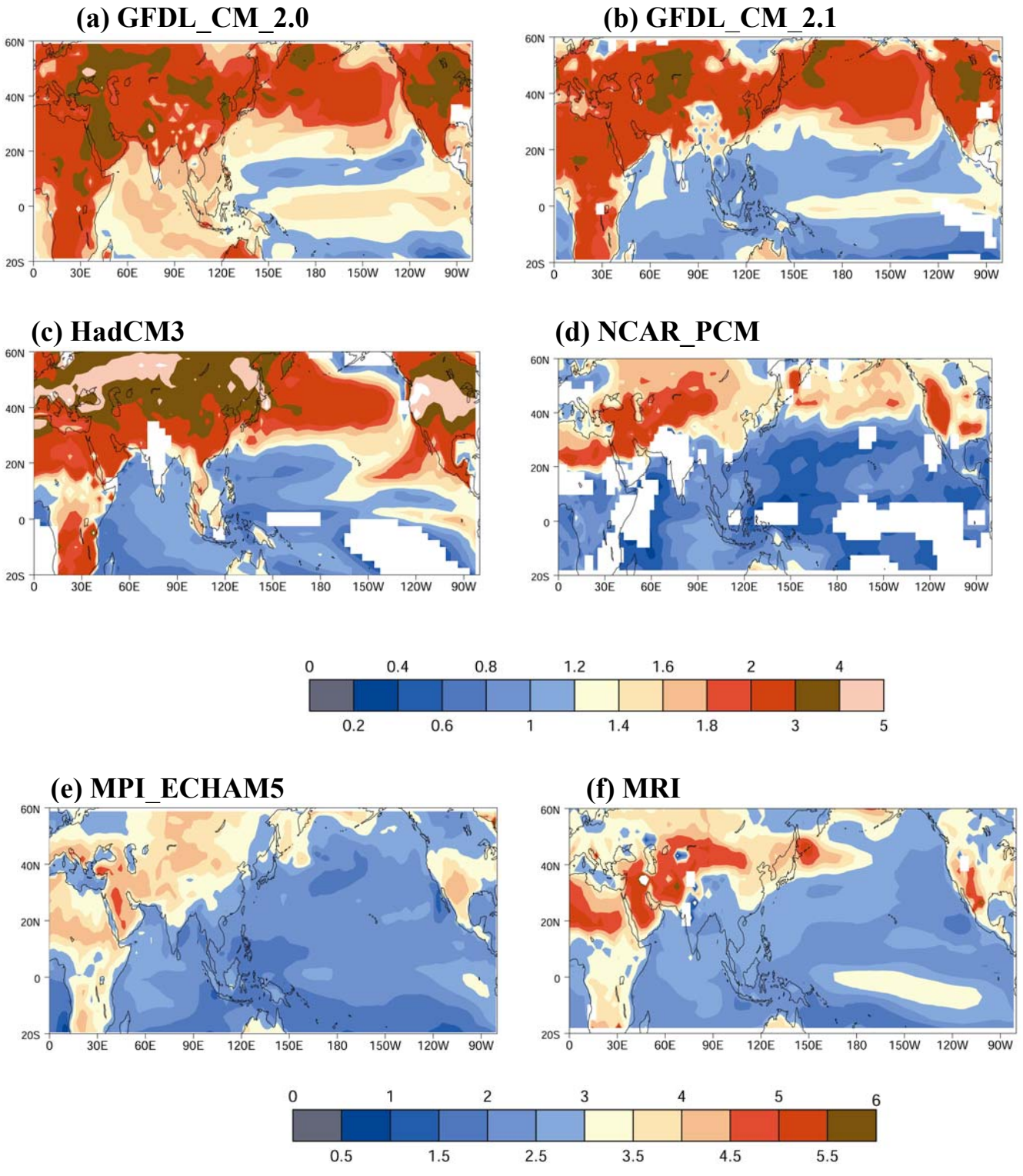

Figure 6: Surface temperature difference (^{o}C; June-September) between the 1pctto2x and 20c3m integrations: (a) GFDL_CM_2.0, (b) GFDL_CM_2.1, (c) HadCM3, (d) NCAR_PCM, (e) MPI_ECHAM5, and (f) MRI. The shading interval is different for the last panels. Only values greater 99% significance level are shown.

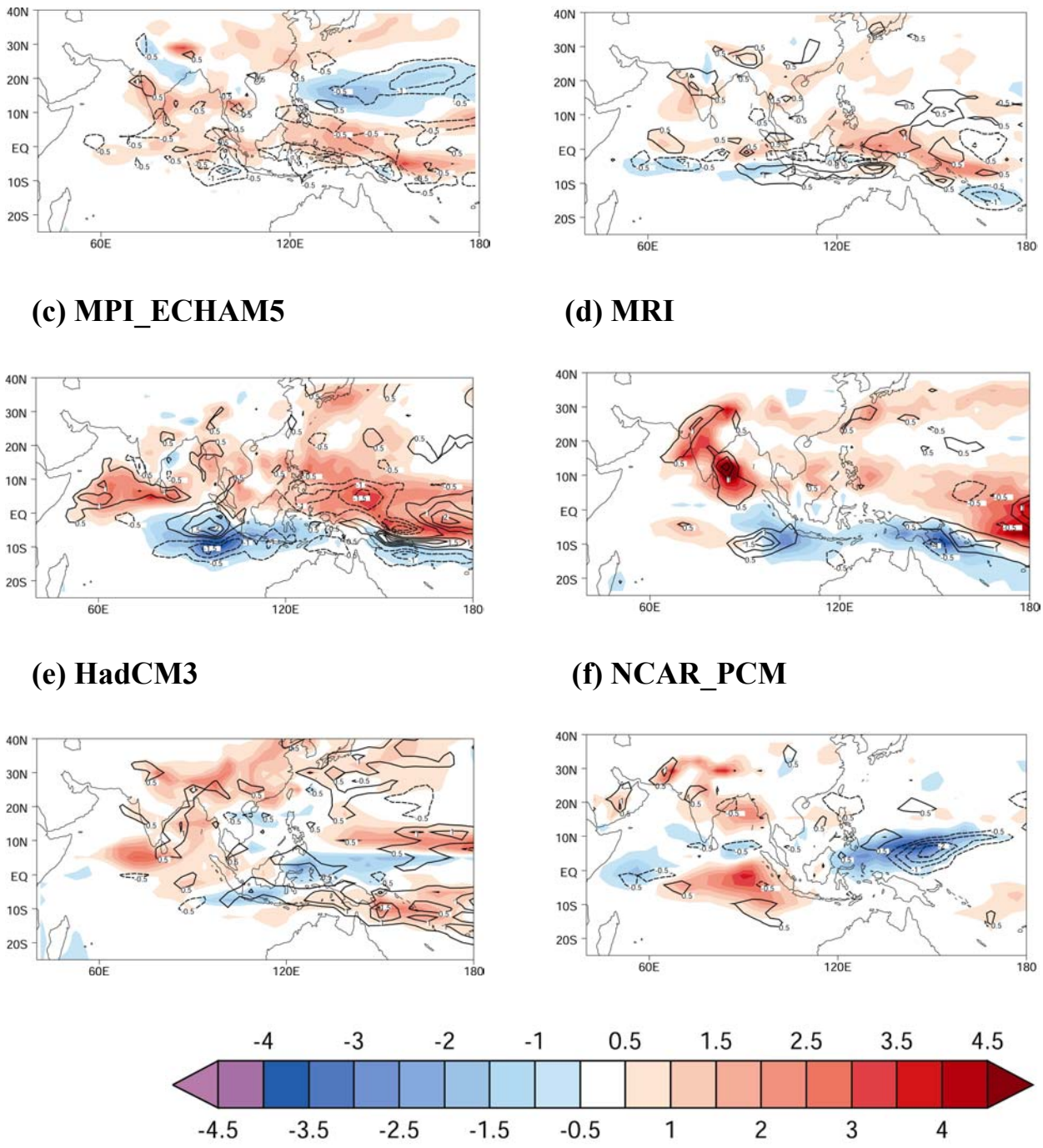

Figure 7: Difference in precipitation (shaded) and standard deviations in precipitation (contours) between 1pctto2x and 20c3m integrations (June-September): (a) GFDL_CM_2.0, (b) GFDL_CM_2.1, (c) MPI_ECHAM5, (d) MRI, (e) HadCM3 and (f) NCAR_PCM. The contour interval is (0.5 mm/day). Values are significant at 90% level (except for MRI in which the values are significant at 95% level).

(a) GFDL_CM_2.0

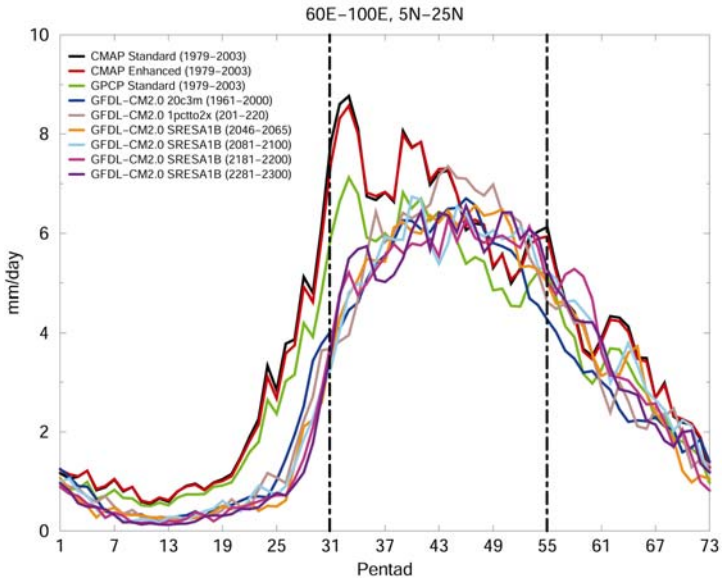

(b) MRI

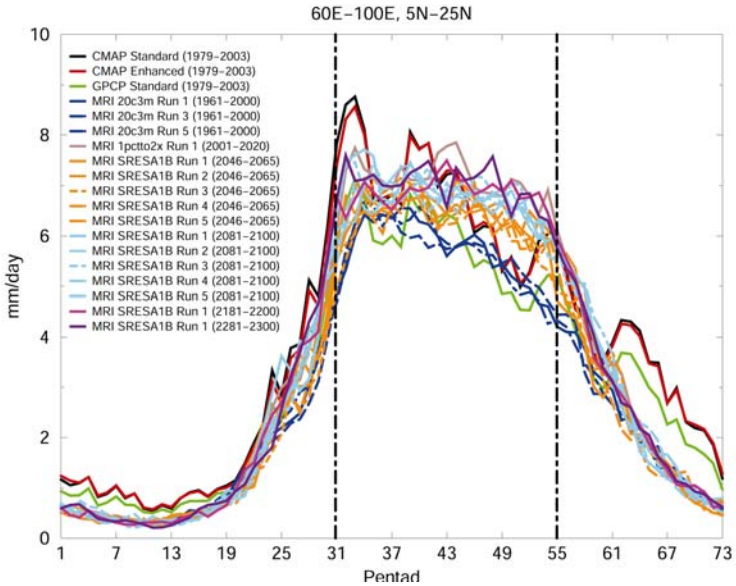

Figure 8: Temporal evolution of pentad mean precipitation averaged over the south Asian monsoon region (60^{o}E-100^{o}E, 5^{o}N-25^{o}N) for: (a) GFDL_CM_2.0 and (b) MRI. The annual cycle is based on the 40-year climatology (1961-2000 for control) and various sub-periods for the SRESA1B experiments, and also from the 1pctto2x integrations. For comparison, the mean annual cycle constructed from three different observed products are also shown. The pentads between the vertical lines correspond to the monsoon season (June-September).

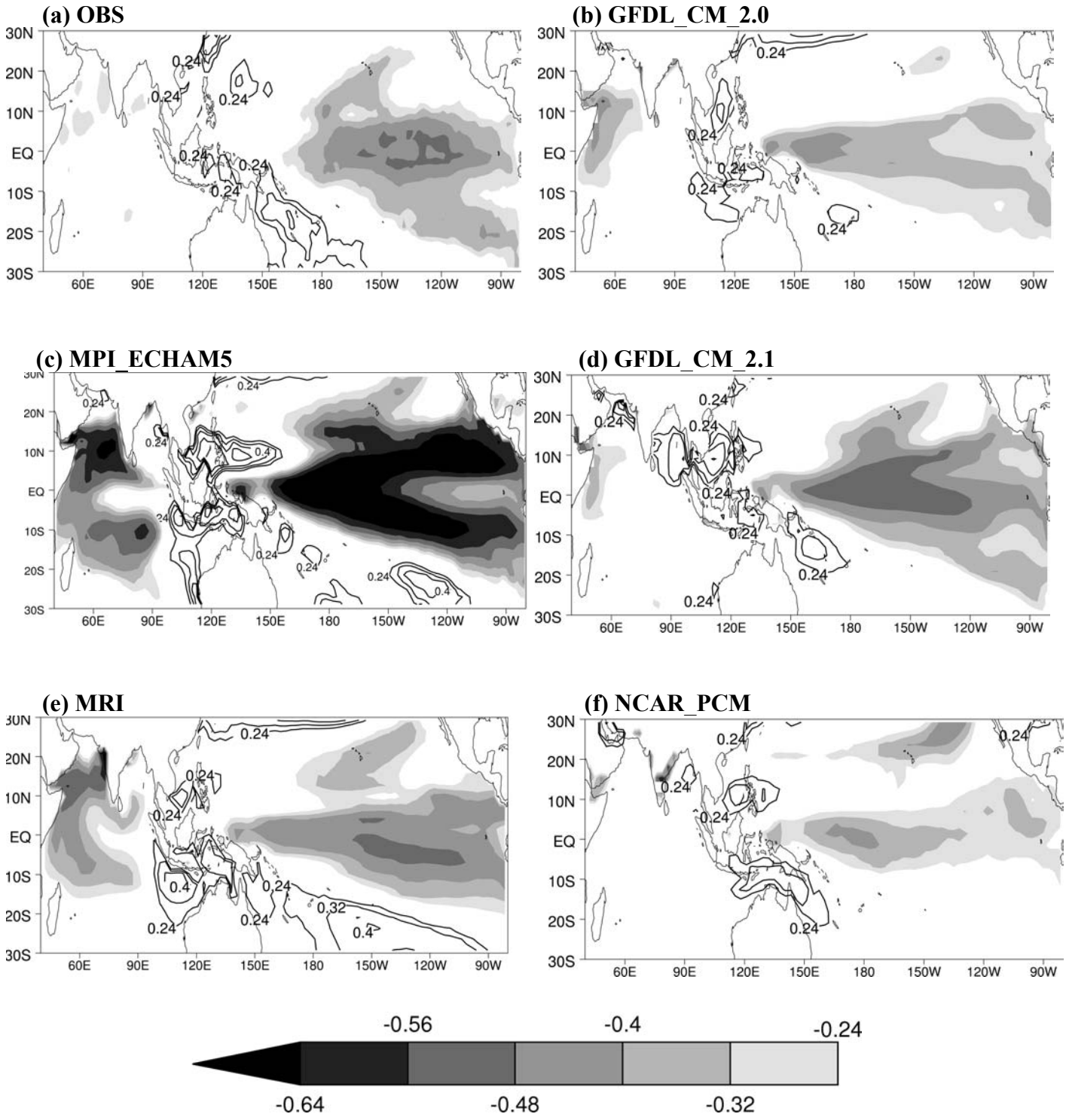

Figure 9: Correlation patterns between seasonal mean (June – September) between AIR indices and sea surface temperature (SST) anomalies from the 20c3m simulations: (a) Observations, (b) GFDL_CM_2.0, (c) MPI_ECHAM5, (d) GFDL_CM_2.1, (e) MRI, and (f) NCAR_PCM. Values significant at greater than 95% level are only shown. Negative (positive) values are shaded progressively (shown as contour with an interval of 0.08).

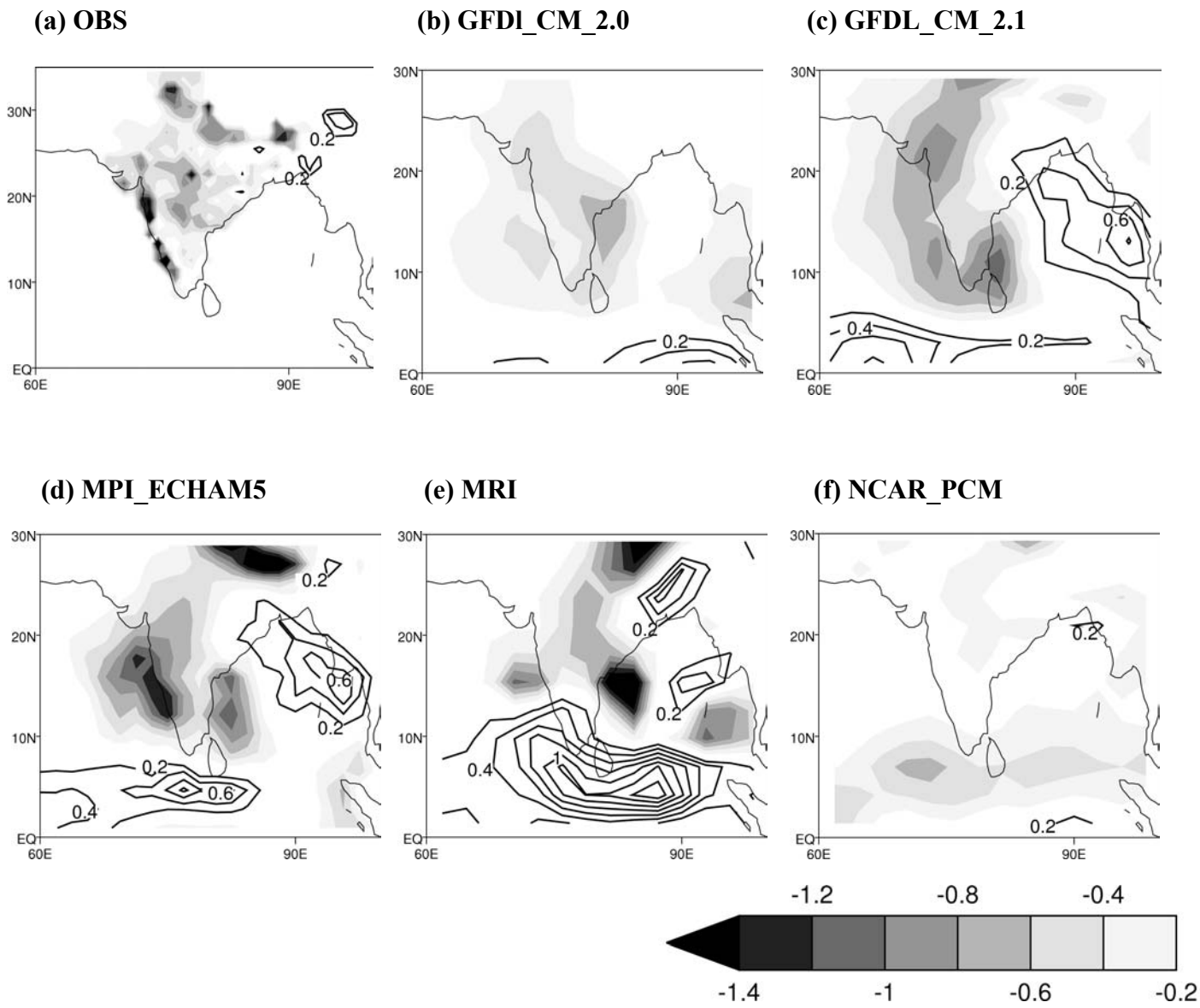

Figure 10: Regression patterns between seasonal mean (June – September) NINO3.4 SST indices and precipitation anomalies (*mm/day*) from the 20c3m simulations: (a) Observations, (b) GFDL_CM_2.0, (c) GFDL_CM_2.1, (d) MPI_ECHAM5, (e) MRI, and (f) NCAR_PCM. Values significant at greater than 95% level are only shown. Negative (positive) values are shaded progressively (shown as contour with an interval of 0.2). All regressions have been scaled by a one standard deviation perturbation of NINO3.4 SST.

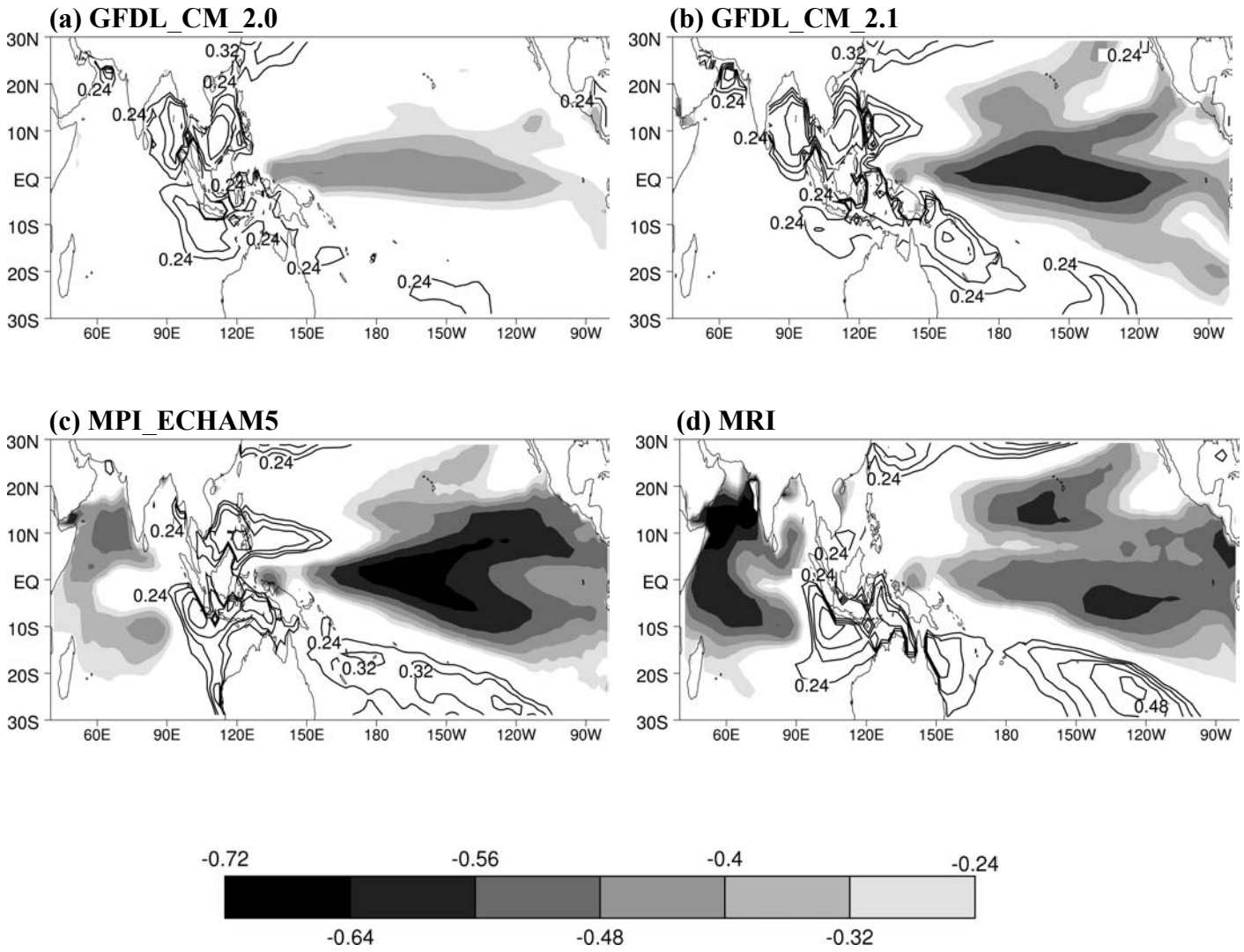

Figure 11: Same as Fig. 7 but for 1pctto2x integrations

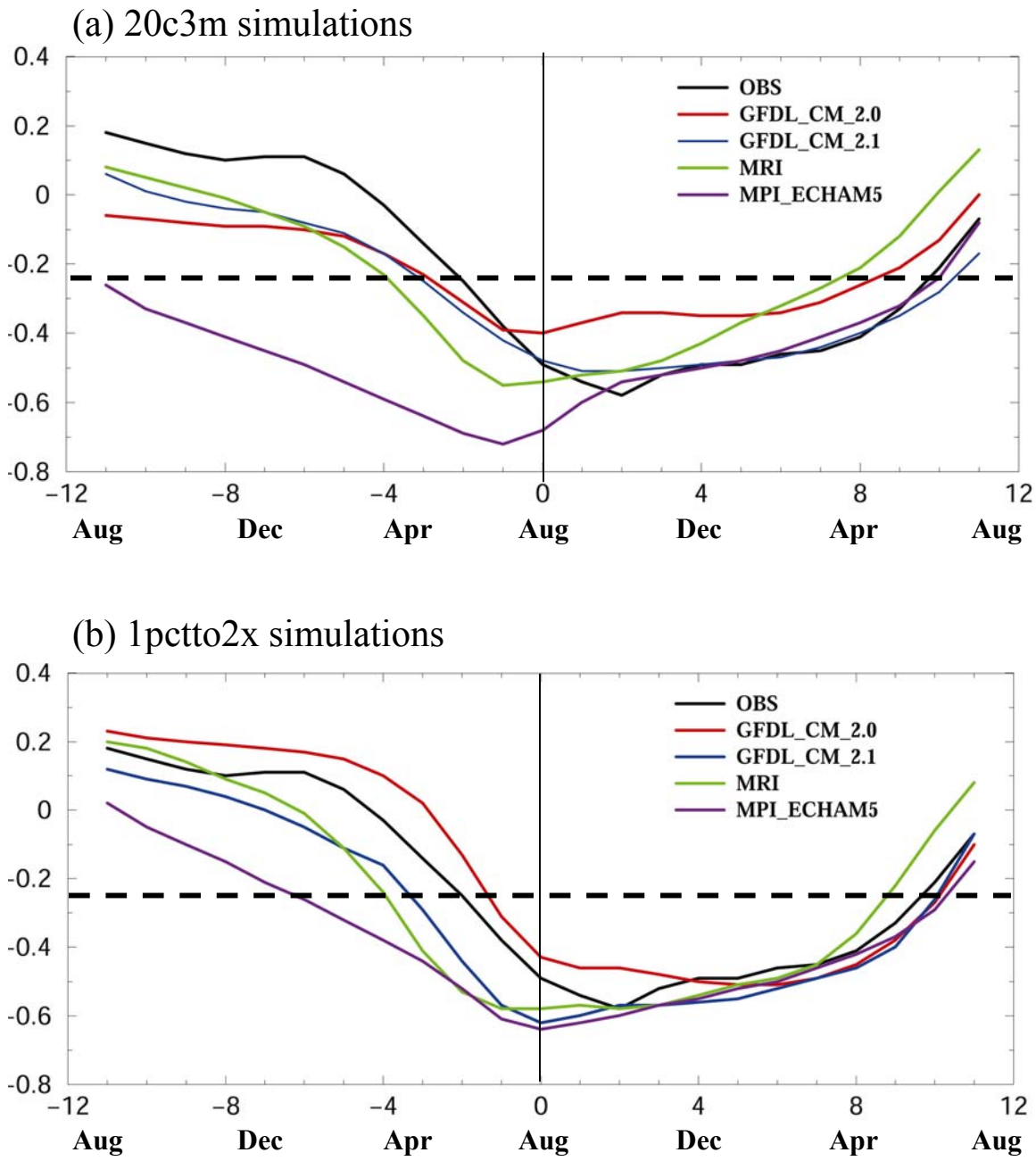

Figure 12: Lag/lead correlation between AIR anomalies and NINO3.4 SST anomalies: (a) 20c3m, and (b) 1pctto2x simulations. In both panels, the results from observations are also shown. Horizontal dotted lines represent the 5% significance level. Lag –12 corresponds to NINO3.4 SST anomalies one year before the monsoon season.

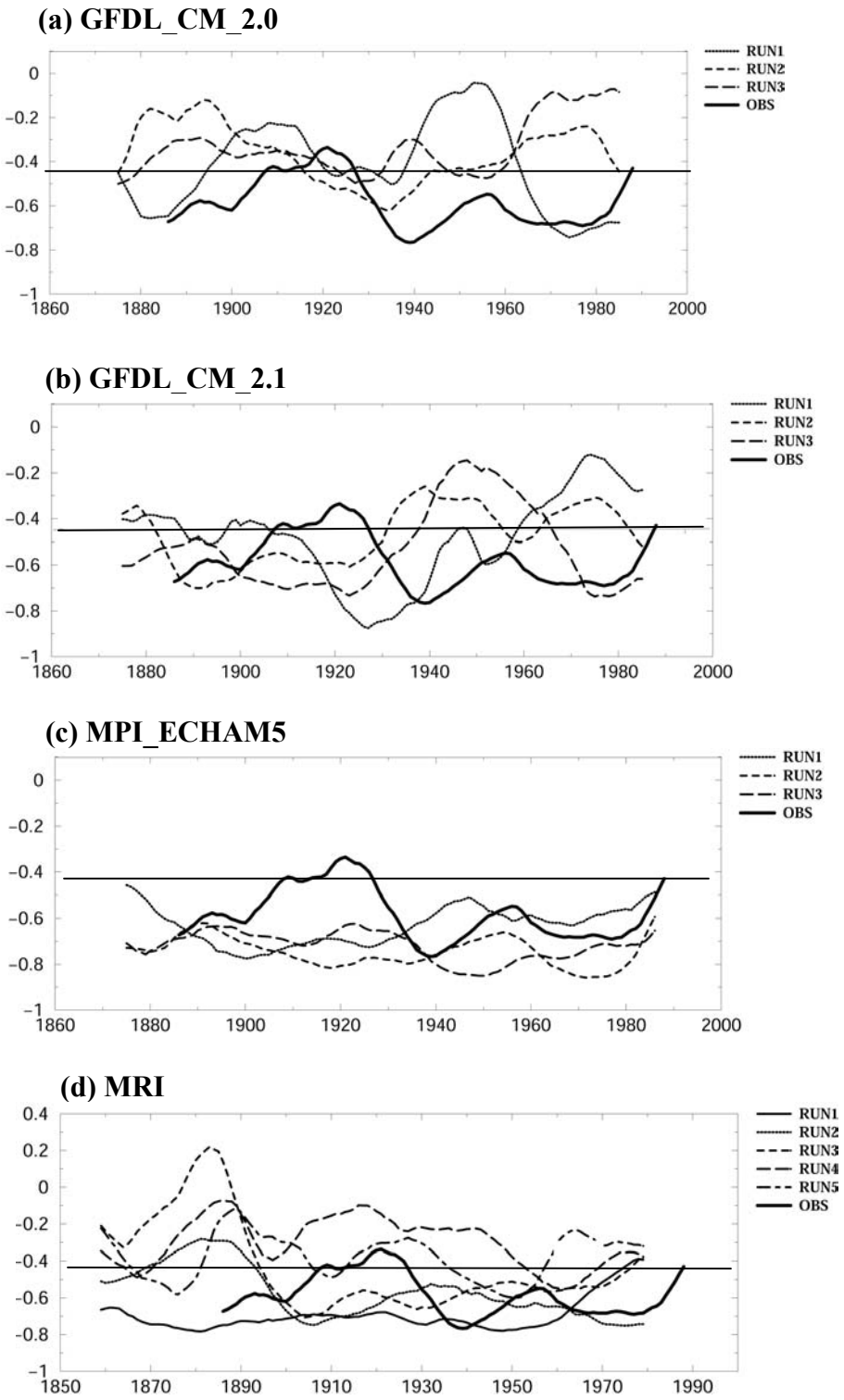

Figure 13: Shown are 21-year sliding correlations between all-India rainfall (AIR) and NINO3.4 SST anomalies (JJAS) for the individual realizations: (a) GFDL_CM_2.0, (b) GFDL_CM_2.1, (c) MPI_ECHAM5, (d) MRI. In all the panels, results from observation are also shown. The horizontal line shows the 5% significance level.

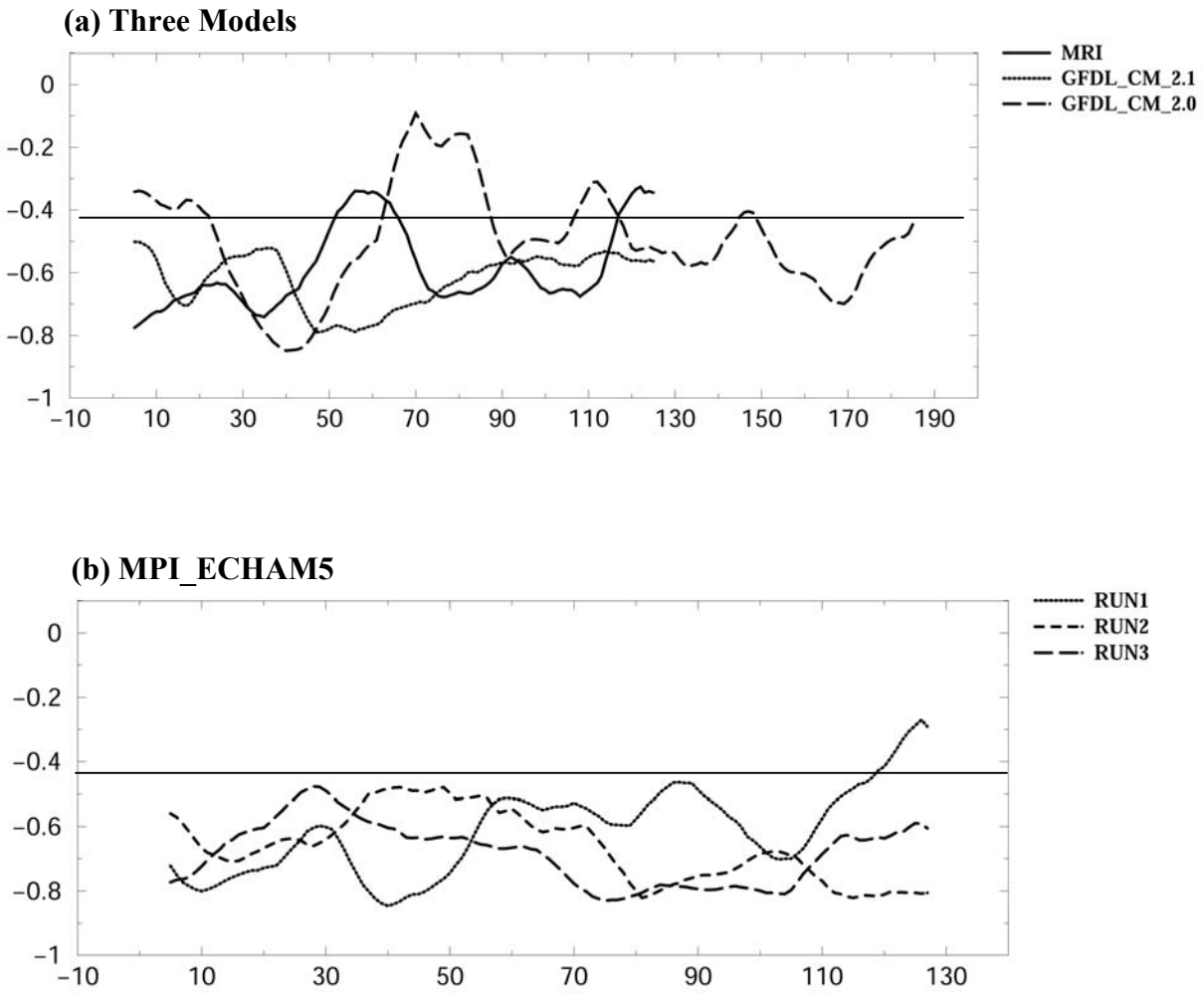

Figure 14: Same as Fig. 11 but from the 1pctto2x runs: (a) single realization from the three models, and (b) three realizations from MPI_ECHAM5. The horizontal lines represent the 5% significance level.

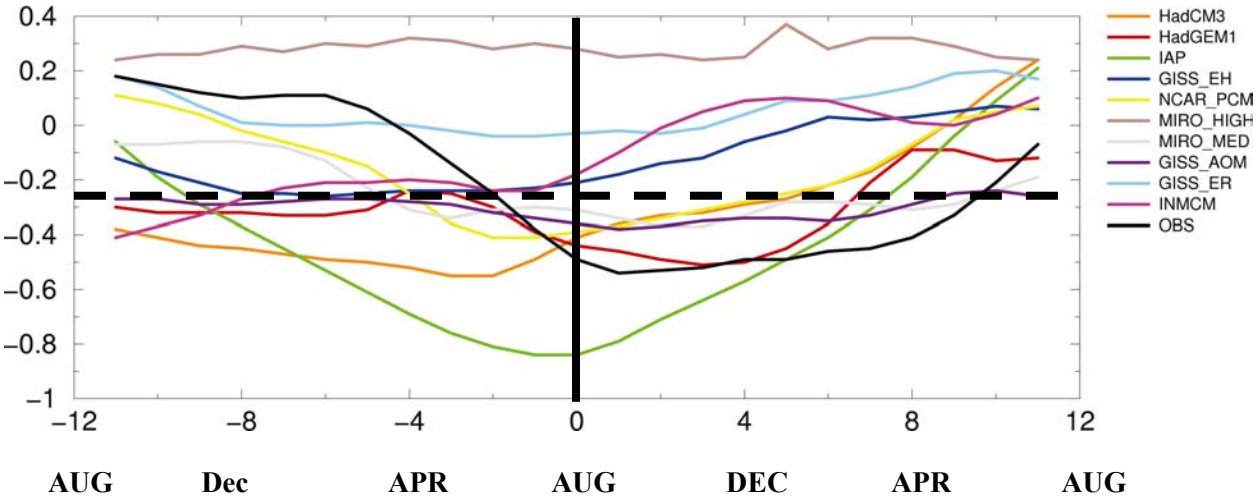

Figure 15: Same as Fig. 12a but for models that have either poor monsoon precipitation climatology and/or unrealistic representation of ENSO variability. Horizontal dotted line represents the 5% significance level. Lag –12 corresponds to Nino3.4 SST anomalies one year before the monsoon season.

Table 1: Given are the modelling group, the model designations, the horizontal and vertical resolution of the atmospheric model and ocean model.

Modelling Group	Model Designation	AGCM Horizontal/ Vertical Resolution	OGCM Horizontal/ Vertical Resolution
Canadian Centre for Climate Modelling & Analysis	CGCM3.1(T47)	T47 L31	192x96 L29
Météo-France/Centre National de Recherches Météorologiques	CNRM-CM3	T42 L45	180x170 L33
CSIRO Atmospheric Research	CSIRO-Mk3.0	T63 L18	1.875x0.925 L31
Max Planck Institute for Meteorology	ECHAM5/MPI-OM	T63 L32	1x1 L42
US Dept. of Commerce/NOAA Geophysical Fluid Dynamics Laboratory	GFDL-CM2.0 GFDL-CM2.1	N45 L24 N45 L24	1x0.33-1 L50 1x0.33-1 L50
NASA / Goddard Institute for Space Studies	GISS-AOM GISS-EH GISS-ER	90x60 L12 72x46 L17 72x46 L17	90x60 L16 2x2 cos(lat) L16 72x46 L13
LASG/Institute of Atmospheric Physics	FGOALS-g1.0	128x60 L26	360x170 L33
Institute for Numerical Mathematics	INM-CM3.0	4x5 L21	2x2.5 L33
Institut Pierre Simon Laplace	IPSL-CM4	96x72 L19	2x2 L31
Center for Climate System Research (The University of Tokyo), National Institute for Environmental Studies, and Frontier Research Center for Global Change (JAMSTEC)	MIROC3.2(hires) MIROC3.2(medres)	T106 L56 T42 L20	T106 L48 256x192 L44
Meteorological Research Institute	MRI-CGCM2.3.2	T42 L30	2x0.5-2.5 L23
National Center for Atmospheric Research	PCM	T42 L18	384x288 L32
Hadley Centre for Climate Prediction and Research/Met Office	UKMO-HadCM3 UKMO-HadGEM1	2.5x3.75 N96 L38	1.25x1.25 L20 1x0.33-1 L40

Table 2 The mean and interannual variability of all-India rainfall (AIR) from the 20th century and $2xCO_2$ integrations. The changes in mean (**t**-test) and variability (**f**-test) are statistically significant. The values are shown for those models that have realistic ENSO-monsoon relationship.

Models	Number of realizations in the 20c3m and length of integrations	Number of realizations in the $2xCO_2$ and length of integrations	Mean AIR in 20c3m (mm)	Mean AIR in $2xCO_2$ (mm)	Interannual Variability of AIR in 20c3m (mm)	Interannual Variability of AIR in $2xCO_2$ (mm)
GFDL_CM_2.0	3 (1861-2000)	1 (280 years)	665.1	735.0	72.00	81.6
GFDL_CM_2.1	3 (1861-2000)	1 (220 years)	853.5	888.9	62.4	69.6
MPI_ECHAM5	3 (1860-2000)	3 (221 years)	661.5	763.5	78.0	96.0
MRI	5 (1851-2000)	1 (220 years)	475.5	645.0	54.0	78.0